

# Beyond Pinball Loss: Quantile Methods for Calibrated Uncertainty Quantification

Youngseog Chung  
Carnegie Mellon University  
youngsec@cs.cmu.edu

Willie Neiswanger  
Stanford University  
neiswanger@cs.stanford.edu

Ian Char  
Carnegie Mellon University  
ichar@cs.cmu.edu

Jeff Schneider  
Carnegie Mellon University  
schneide@cs.cmu.edu

## Abstract

Among the many ways of quantifying uncertainty in a regression setting, specifying the full quantile function is attractive, as quantiles are amenable to interpretation and evaluation. A model that predicts the true conditional quantiles for each input, at all quantile levels, presents a correct and efficient representation of the underlying uncertainty. To achieve this, many current quantile-based methods focus on optimizing the so-called *pinball loss*. However, this loss restricts the scope of applicable regression models, limits the ability to target many desirable properties (e.g. calibration, sharpness, centered intervals), and may produce poor conditional quantiles. In this work, we develop new quantile methods that address these shortcomings. In particular, we propose methods that can apply to any class of regression model, allow for selecting a Pareto-optimal trade-off between calibration and sharpness, optimize for calibration of centered intervals, and produce more accurate conditional quantiles. We provide a thorough experimental evaluation of our methods<sup>1</sup>, which includes a high dimensional uncertainty quantification task in nuclear fusion.

## 1 Introduction

Uncertainty quantification (UQ) in statistics and machine learning refers to quantifying the confidence of a prediction. This measure of certainty can be crucial in a variety of downstream applications, including Bayesian optimization (Shahriari et al. [2015], Mockus et al. [1978]), model-based reinforcement learning (Yu et al. [2020], Malik et al. [2019], Chua et al. [2018], Garcia and Fernández [2012]), and in high-stakes predic-

tions where mistakes incur large costs (Rudin [2019], Wexler [2017]).

While the common goal of UQ is to describe the full predictive distribution of the outputs given an input, the representation of the distributional prediction is varied across different methods. Some methods assume a parametric distribution and return parameter estimates (Zhao et al. [2020], Detlefsen et al. [2019], Lakshminarayanan et al. [2017]), while others return density function estimates, as is commonly done in Bayesian methods (Maddox et al. [2019], Liu et al. [2019], Hernández-Lobato and Adams [2015], Blundell et al. [2015], Koller and Friedman [2009], Rasmussen [2003]). Alternatively, many methods represent predictive uncertainty with quantile estimates (Salem et al. [2020], Tagasovska and Lopez-Paz [2019], Pearce et al. [2018a]).

Quantiles provide an attractive representation for uncertainty because they can be used to model complex distributions without parametric assumptions, are interpretable with units in the target output space, allow for easy construction of prediction intervals, and can be used to efficiently sample from the predictive distribution via inverse transform sampling (Hao et al. [2007], Koenker and Hallock [2001]). Learning the quantile for a single quantile level is a well studied problem in quantile regression (QR) (Koenker and Hallock [2001], Koenker [2005]), which typically involves optimizing the so-called *pinball loss*, a tilted transformation of the absolute value function. By training for all quantiles simultaneously, recent works have made concrete steps in incorporating QR methods to form competitive UQ methods which output the full predictive distribution (Rodrigues and Pereira [2020], Tagasovska and Lopez-Paz [2019]).

In this work, we highlight some limitations of the pinball loss and propose several methods to address these shortcomings. Specifically, we explore the following:

- **Model agnostic QR.** Optimizing the pinball loss often restricts the choice of model family for

<sup>1</sup>Code is available at <https://github.com/YoungseogChung/calibrated-quantile-uq>.

which we can provide UQ. We propose an algorithm to learn all quantiles simultaneously by utilizing methods from conditional density estimation. This algorithm is agnostic to model class and can be applied to *any* regression model.

- **Trading off calibration and sharpness.** On its own, pinball loss does not directly target calibration and sharpness, even though these are important quantities for model evaluation. We propose a tunable loss function that targets these quantities directly and show empirically that the trained model can trade-off between calibration and sharpness Pareto-optimally.
- **Centered intervals.** In practice, we often desire uncertainty predictions made with centered intervals, which are not produced when optimizing the pinball loss. We propose an alternative loss function that is better suited for this goal.
- **Encouraging individual calibration.** Perfect quantile forecasts will satisfy *individual* calibration, which is a much stricter condition than the notion of calibration commonly used (i.e. average calibration). We introduce a training procedure that aims to improve quantile predictions beyond average calibration, and demonstrate its efficacy via *adversarial group* calibration.

We proceed by first laying out relevant metrics used to assess the quality of predictive UQ, and discuss the pitfalls of optimizing the pinball loss (Section 2). Drawing motivation from Section 2, we present our proposed methods in Section 3. In Section 4, we demonstrate our methods experimentally, where we model predictive uncertainty on benchmark datasets, and on a high-dimensional, real-world uncertainty estimation task from nuclear fusion.

## 2 Preliminaries and Background

### 2.1 Notation and Terms

Bold upper case letters  $\mathbf{X}, \mathbf{Y}$  denote random variables, lower case letters  $x, y$ , denote specific values, and calligraphic upper case letters  $\mathcal{X}, \mathcal{Y}$  denote the set of possible values. We always consider  $x \in \mathcal{X}$  to be the input feature vector and  $y \in \mathcal{Y}$  to be the corresponding target. Additionally, we consider the regression setting where  $\mathcal{Y} \subset \mathbb{R}$  and  $\mathcal{X} \subset \mathbb{R}^n$ . We use  $\mathbb{F}_{\mathbf{X}}, \mathbb{F}_{\mathbf{Y}|x}, \mathbb{F}_{\mathbf{Y}}$  to denote the true cumulative distribution of the subscript random variable. For any  $x \in \mathcal{X}$ , we assume there exists a true conditional distribution  $\mathbb{F}_{\mathbf{Y}|x}$  over  $\mathcal{Y}$ , and we assume  $\mathbb{Q}(x, p)$  to be the true  $p^{\text{th}}$  quantile of this distribution, i.e.  $\mathbb{F}_{\mathbf{Y}|x}(\mathbb{Q}(x, p)) = p$ . Any estimates of the true functions  $\mathbb{F}, \mathbb{Q}$  will be denoted with a hat,  $\hat{\mathbb{F}}, \hat{\mathbb{Q}}$ . We will specifically refer to any model

of  $\mathbb{Q}, \hat{\mathbb{Q}} : \mathcal{X} \times (0, 1) \rightarrow \mathcal{Y}$ , as a “quantile model”. Lastly, unless otherwise noted, we will always consider the *conditional* problem of estimating quantities in the target space  $\mathcal{Y}$ , conditioned on a value  $x \in \mathcal{X}$ .

### 2.2 Metrics for Assessing UQ Quality

While various metrics have been used in literature to assess the quality of UQ, there has been a great deal of recent focus on the notions of *calibration* and *sharpness* (Zhao et al. [2020], Tran et al. [2020], Kuleshov et al. [2018], Guo et al. [2017], Gneiting et al. [2007]).

We introduce the notion of calibration here, but for a more thorough treatment, see Zhao et al. [2020]. Broadly speaking, calibration requires that the probability of observing the target random variable below a predicted  $p^{\text{th}}$  quantile is equal to the *expected probability*  $p$ , for all  $p \in (0, 1)$ . We refer to the former quantity as the *observed probability* and denote it  $p^{\text{obs}}(p)$ , for an expected probability,  $p$ . We will often drop the reliance on  $p$  and simply write  $p^{\text{obs}}$  when it is clear from context. Calibration requires  $p^{\text{obs}}(p) = p, \forall p \in (0, 1)$ . From this generic statement, we can describe different notions of calibration based on how  $p^{\text{obs}}$  is defined.

A model is **individually calibrated** if it outputs the true conditional quantiles, i.e.  $\hat{\mathbb{Q}}(x, p) = \mathbb{Q}(x, p)$ . In this case, we define the observed probability to be

$$p_{\text{indv}}^{\text{obs}}(p, x) := \mathbb{F}_{\mathbf{Y}|x}(\hat{\mathbb{Q}}(x, p)), \forall x \in \mathcal{X}, \forall p \in (0, 1). \quad (1)$$

In words, this requires that the probability of observing  $y$  below the quantile prediction be equal to  $p$ , at each point  $x \in \mathcal{X}$ , *individually*. If we can verify this property for all  $x \in \mathcal{X}$ , then by definition, we will know the quantile output is correct and precisely the true conditional quantile. However, individual calibration is unverifiable with finite datasets in the assumption-less case. This is because a dataset usually contains at most one  $y$  value for any  $x$  value (Zhao et al. [2020]).

A relaxed condition is **average calibration**. In this case, we define the observed probability to be

$$p_{\text{avg}}^{\text{obs}}(p) := \mathbb{E}_{x \sim \mathbb{F}_{\mathbf{X}}}[\mathbb{F}_{\mathbf{Y}|x}(\hat{\mathbb{Q}}(x, p))], \forall p \in (0, 1), \quad (2)$$

i.e. the probability of observing the target below the quantile prediction, *averaged over*  $\mathbb{F}_{\mathbf{X}}$ , is equal to  $p$ . This is identical to requiring individual calibration *on average* over the domain  $\mathcal{X}$ . Average calibration is often referred to simply as “calibration” (Kuleshov et al. [2018]), and is a commonly used metric because it can be estimated with finite datasets. Given a dataset with  $N$  points,  $\{(x_i, y_i)\}_{i=1}^N$ , we can estimate average calibration using

$$\hat{p}_{\text{avg}}^{\text{obs}}(p) = \frac{1}{N} \sum_{i=1}^N \mathbb{I}\{y_i \leq \hat{\mathbb{Q}}(x_i, p)\}. \quad (3)$$

Note that if our quantile estimate achieves average calibration then  $\hat{p}_{avg}^{obs} \rightarrow p$  as  $N \rightarrow \infty$ ,  $\forall p \in (0, 1)$ . The degree of error in average calibration is commonly measured by *expected calibration error* (ECE), i.e.

$$ECE = \int_0^1 |p_{avg}^{obs}(p) - p| dp. \quad (4)$$

While an individually calibrated model is also average calibrated, it may be possible to have an uninformative, yet average calibrated model. For example, quantile predictions that match the true *marginal* quantiles of  $\mathbb{F}_{\mathbf{Y}}$  will be average calibrated, but will hardly be useful because they do not consider the input  $x$  at all.

Therefore, the notion of **sharpness** is often considered together with average calibration. There generally exists a tradeoff between average calibration and sharpness (Murphy [1973], Gneiting et al. [2007]). Sharpness calls for tight distributional predictions; for example, in predictions that parameterize a Gaussian, the variance of the predicted distribution is often taken as a measure of sharpness. In non-parametric predictions, the width of a centered 95% prediction interval is a commonly used proxy.

Recent works have suggested a notion of calibration stronger than average calibration, called adversarial group calibration (Zhao et al. [2020]). This stems from the notion of **group calibration** (Hébert-Johnson et al. [2017], Kleinberg et al. [2016]), which prescribes measurable subsets  $\mathcal{S}_i \subset \mathcal{X}$  s.t.  $P_{x \sim \mathbb{F}_{\mathbf{X}}}(x \in \mathcal{S}_i) > 0$ ,  $i = 1, \dots, k$ , and requires the predictions to be average calibrated within each subset,  $\mathcal{S}_1, \dots, \mathcal{S}_k$ . Adversarial group calibration does not prescribe known subsets in advance, but requires average calibration for *any subset of  $\mathcal{X}$  with non-zero measure*. Denote  $\mathbf{X}_{\mathcal{S}}$  as a random variable that is conditioned on being in the set  $\mathcal{S}$ . For **adversarial group calibration**, the observed probability is

$$p_{adv}^{obs}(p) := \mathbb{E}_{x \sim \mathbb{F}_{\mathbf{X}_{\mathcal{S}}}}[\mathbb{F}_{\mathbf{Y}|x}(\hat{Q}(x, p))], \forall p \in (0, 1), \quad (5)$$

$$\forall \mathcal{S} \subset \mathcal{X} \text{ s.t. } P_{x \sim \mathbb{F}_{\mathbf{X}}}(x \in \mathcal{S}) > 0.$$

With a finite dataset, we can measure a proxy of adversarial group calibration by measuring the average calibration within all subsets of the dataset with sufficiently many points.

The key difference among the three notions of calibration is the distribution over input points. Individual calibration inspects the discrepancy between observed and expected probabilities for individual inputs  $x \in \mathcal{X}$ , where any single point  $x$  has probability measure 0. Adversarial group calibration relaxes this by similarly inspecting any subset of  $\mathcal{X}$  with non-zero measure. Average calibration relaxes this further by considering the whole distribution of  $\mathbf{X}$ .

One alternative family of evaluation metrics is **proper scoring rules** (Gneiting and Raftery [2007]). Proper scoring rules are summary statistics of overall performance of a distributional prediction, which consider both calibration and sharpness jointly (Gneiting et al. [2007]). For example, negative log-likelihood (NLL) is a proper scoring rule that is commonly used with density predictions (Detlefsen et al. [2019], Pearce et al. [2018b], Lakshminarayanan et al. [2017]). For quantile predictions, one proper score is the **check score**, which is identical to the pinball loss. This gives more ground to optimizing the pinball loss, which is the traditional method in quantile regression (Koenker and Bassett Jr [1978]), and recent quantile-based UQ methods focus on optimizing the pinball loss (Rodrigues and Pereira [2020], Tagasovska and Lopez-Paz [2019], Cannon [2018], Xu et al. [2017]).

The minimum of the expectation of the pinball loss is attained at the true conditional quantile. However, for finite datasets, we can show that minimizing the pinball loss does not necessarily lead to average calibration on the dataset.

**Proposition 1** Consider a dataset  $D = \{(x_i, y_i)\}_{i=1}^N$  with unique  $x_i \in \mathcal{X}$ , model class  $F$  with an infinite capacity, and pinball loss  $\rho_{\tau}(y, \hat{y}) = (\hat{y} - y)(\mathbb{I}\{y \leq \hat{y}\} - \tau)$ . For any level  $\tau \in [0, 1]$ , the minimizer  $\argmin_{f \in F} \left[ \sum_{i=1}^N \rho_{\tau}(y_i, f(x_i)) \right]$  achieves 0 pinball loss. However, these minimizers yield a miscalibrated uncertainty prediction with  $ECE = 0.5$ .

We prove Proposition 1 in Appendix A.1. At first glance, this proposition may not be surprising since overfitting is an inherent problem that one needs to account for in most machine learning problems. The key difference here is the magnitude of the problem that overfitting causes. By achieving perfect pinball loss, one is left with an inaccurate UQ model that is highly miscalibrated, even on the training dataset.

The intuition is that the pinball loss implicitly decides a balance between calibration and sharpness based on the expressivity of the model class. With high-capacity models such as neural networks (NNs), the pinball loss unequally favors sharpness over calibration. Hence, in practice, when using the pinball loss, the correct balance between calibration and sharpness depends on either choosing the correct class of models with an appropriate level of capacity, or applying the correct amount of constraint or regularization on a chosen model class, both of which may be very difficult to specify with arbitrary function approximators (e.g. NNs). These pitfalls motivate our loss function in Section 3.2, which explicitly selects a trade-off between calibration and sharpness.

### 3 Methods

#### 3.1 Utilizing Conditional Density Estimation for Model Agnostic QR

One drawback of many existing quantile-based UQ methods is that their training procedure requires differentiable models. In fact, most UQ methods depend on using a specific class of models because of their modeling structure or their loss objective (e.g. Gaussian processes (Rasmussen [2003]), dropout (Gal and Ghahramani [2016]), latent variable models (Koller and Friedman [2009]), simultaneous pinball loss (Tagasovska and Lopez-Paz [2019]), and NLL-based losses (Lakshminarayanan et al. [2017])).

This model restriction can be especially unfavorable in practical settings. A domain expert with an established point prediction model and compute infrastructure may want to add uncertainty quantifications without a great deal of additional overhead. To address these issues, we can consider the following model-agnostic procedure. Instead of optimizing a designated loss function, we can consider splitting the given problem into two parts: estimating the conditional quantiles directly from data, then regressing onto these estimates. The benefit of this method is that, granted we can estimate the conditional quantiles accurately, we can use any regression model to predict these quantile estimates. Further, this regression task directly targets the goal of producing the conditional quantiles (i.e. for individual calibration). This procedure, which we refer to as *Model Agnostic QR* (MAQR), is outlined in Algorithm 1.

---

**Algorithm 1** Model Agnostic Quantile Regression
 

---

- 1: **Input:** Train data  $\{x_i, y_i\}_{i=1}^N$ , trained regression model  $\hat{f}(x)$
  - 2: Calculate the residuals  $\epsilon_i = y_i - \hat{f}(x_i)$ ,  $i \in [N]$
  - 3: Initialize  $D \leftarrow \emptyset$
  - 4: **for**  $i = 1$  **to**  $N$  **do**
  - 5:    $E_{i,d} \leftarrow \{\epsilon_j : \text{dist}(x_i, x_j) \leq d, 1 \leq j \leq N\}$
  - 6:   Construct an empirical CDF with  $E_{i,d}$  to produce  $\hat{\mathbb{F}}_{\mathbf{E}|x_i} : \epsilon \mapsto p \in [0, 1]$
  - 7:   Select a set of quantile levels  $\{p_k\}_{k=1}^m$ ,  $p_k \in [0, 1]$
  - 8:    $\hat{q}_{i,p_k} \leftarrow \inf\{\epsilon : p_k \leq \hat{\mathbb{F}}_{\mathbf{E}|x_i}(\epsilon)\}$ ,  $k = 1, \dots, m$
  - 9:    $D \leftarrow D \cup \{x_i, p_k, \hat{q}_{i,p_k}\}_{k=1}^m$
  - 10: **end for**
  - 11: Use  $D$  to fit a regression model  $\hat{g}$   
 $\hat{g} : (x_i, p_k) \mapsto \hat{q}_{i,p_k}$ ,  $k = 1, \dots, m$
  - 12: **Output:**  $\hat{f} + \hat{g}$ ,  $k = 1, \dots, m$
- 

This algorithm is based on the *key assumption* that nearby points in  $\mathcal{X}$  will have similar conditional distributions, i.e. if  $x_j \approx x_k$  then  $\mathbb{F}_{\mathbf{Y}|x_j} \approx \mathbb{F}_{\mathbf{Y}|x_k}$ . With this assumption about the smoothness of conditional dis-

tributions over  $\mathcal{X}$ , we can construct groups of neighboring points to estimate the conditional density, at each locality over  $\mathcal{X}$ . This locality is determined by the hyperparameter  $d$  in line 5. The conditional density is estimated with an empirical CDF of the group of neighboring points, and conditional quantile estimates are made with this empirical CDF. These conditional quantile estimates are collected into  $D$ , which is ultimately used as the training set for our quantile model,  $\hat{g}$ . In practice, we perform all of these steps with the *residuals* by first estimating a mean function,  $\hat{f}$  (line 2), which produces more accurate empirical CDFs. This method takes advantage of the fact that accurate point prediction models often already exist in many application settings.

Algorithm 1 is a specific implementation of a more general model-agnostic algorithm, in which we can directly estimate conditional quantiles from the data with tools from conditional density estimation, and regress onto these estimates. We note that using KDEs for conditional density estimation is a well studied problem with theoretical guarantees on consistency (Holmes et al. [2012], Hyndman et al. [1996], Stute et al. [1986]). In Appendix A.2, we state the general form of Algorithm 1, and show how our quantile estimation procedure falls under the guarantees stated by Stute et al. [1986]. As we will demonstrate in Section 4, basing predictions on these density estimates sidesteps the issues inherent to pinball loss.

#### 3.2 Trading off calibration for sharpness with the penalized calibration loss

While MAQR can produce strong results, its performance can suffer in high-dimensional settings, where nonparametric conditional density estimation methods also falter. Neural networks (NNs) have shown good performance in high dimensional settings, given their high capacity to approximate complex functions and recent advances in fast gradient-based optimization. We therefore propose a loss-based approach to estimating conditional quantiles for NNs and other differentiable models.

We draw motivation from the conflict between finite sample average calibration and pinball loss from Section 2.2. Suppose that our explicit goal is to optimize the average calibration, which corresponds to optimizing Equation 3. For any given  $p$ , Equation 3 is non-differentiable because of the indicator function (an estimate of the true CDF). However, one workaround to this is the following:

1. Observe the current coverage  $\hat{p}_{avg}^{\text{obs}}$ .
2. If  $\hat{p}_{avg}^{\text{obs}} < p$ , raise  $\hat{\mathbb{Q}}$  to increase coverage below  $\hat{\mathbb{Q}}$ ;  
 if  $\hat{p}_{avg}^{\text{obs}} > p$ , lower  $\hat{\mathbb{Q}}$  to reduce coverage below  $\hat{\mathbb{Q}}$ .
3. Repeat steps 1, 2 until  $\hat{p}_{avg}^{\text{obs}}$  has converged to  $p$ .



These steps prescribe whether to lower or raise  $\hat{Q}$ , and guide the observed probability,  $\hat{p}_{avg}^{obs}$ , towards  $p$ , thus improving average calibration. Given a finite dataset  $D = \{x_i, y_i\}_{i=1}^N$ , a quantile model  $\hat{Q}$ , and a probability  $p$ , we propose the **calibration loss**

$$\mathcal{C}(D, \hat{Q}, p) =$$

$$\begin{aligned} & \mathbb{I}\{\hat{p}_{avg}^{obs} < p\} \frac{1}{N} \sum_{i=1}^N \left[ (y_i - \hat{Q}(x_i, p)) \mathbb{I}\{y_i > \hat{Q}(x_i, p)\} \right] \\ & + \mathbb{I}\{\hat{p}_{avg}^{obs} > p\} \frac{1}{N} \sum_{i=1}^N \left[ (\hat{Q}(x_i, p) - y_i) \mathbb{I}\{\hat{Q}(x_i, p) > y_i\} \right]. \end{aligned}$$

In words, the calibration loss is calculated as follows: if coverage is lower than desired ( $\hat{p}_{avg}^{obs} < p$ ), then penalize the predictions that are lower than the datapoints by the magnitude of their residuals ( $y_i - \hat{Q}(x_i, p)$ ), and vice versa. We can also scale the loss by the magnitude of miscalibration  $|\hat{p}_{avg}^{obs} - p|$ , which we call **scaled calibration loss**

$$\mathcal{C}_{scaled}(D, \hat{Q}, p) = |\hat{p}_{avg}^{obs} - p| \mathcal{C}(D, \hat{Q}, p) \quad (6)$$

Unlike the pinball loss, even when considering a model with infinite capacity, a minimizer of the calibration loss occurs when the prediction is average calibrated  $\hat{p}_{avg}^{obs} = p$ . However, average calibration is not a sufficient condition for meaningful UQ, hence we also need to consider the *sharpness* of the quantile model.

One instantiation of a sharpness penalty can be to predict the  $(1 - p)^{th}$  quantile  $\hat{Q}(x_i, 1 - p)$  alongside each prediction  $\hat{Q}(x_i, p)$  and penalize the width between these two outputs, using

$$\mathcal{P}(D, \hat{Q}, p) = \frac{1}{N} \sum_{i=1}^N \begin{cases} \hat{Q}(x_i, 1 - p) - \hat{Q}(x_i, p) & (p \leq 0.5) \\ \hat{Q}(x_i, p) - \hat{Q}(x_i, 1 - p) & (p > 0.5) \end{cases}$$

In early training stages, the model output  $\hat{Q}(x, p)$  may not be increasing in  $p$ , hence we penalize only when it is positive. In addition, it's important to note that the true underlying distribution will not have 0 sharpness if there is significant noise. Therefore, we should only penalize sharpness when the data suggests our quantiles are too dispersed, i.e. when  $\hat{Q}(x_i, 1 - p) - \hat{Q}(x_i, p)$ , the coverage in between the quantiles, is greater than  $|2p - 1|$ , the expected coverage.

Combining the calibration and sharpness terms, we have the following minimization objective:

$$\mathcal{L}(D, \hat{Q}, p) = (1 - \lambda) \mathcal{C}(D, \hat{Q}, p) + \lambda \mathcal{P}(D, \hat{Q}, p). \quad (7)$$

By scaling the hyperparameter  $\lambda$  in  $[0, 1]$ , we can trade-off between the calibration and sharpness objectives. This is especially useful when working with real-world

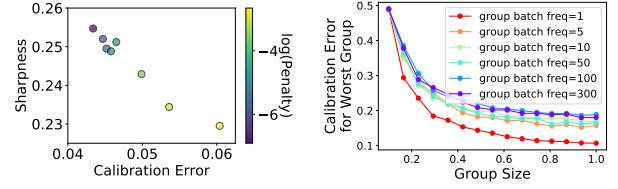


Figure 1: **Left:** By tuning the sharpness penalty coefficient in the combined calibration loss, we can trade-off calibration and sharpness in the prediction. **Right:** Increasing the frequency of group batching epochs (with uniform batching in other epochs) during training also helps SQR (which optimizes pinball loss) achieve better adversarial group calibration.

data. Because it is impossible to verify the exact correctness of the calibration-sharpness pair of a prediction, a practitioner may want to choose to emphasize one aspect over the other, depending on their application (Malik et al. [2019], Murphy [1973]). We show in Figure 1 how scaling  $\lambda$  allows predictions to traverse the calibration-sharpness Pareto front. Since we learn a quantile model  $\hat{Q}$  that outputs the conditional quantile estimates for all probabilities, following Tagasovska and Lopez-Paz [2019], our training objective is:  $\mathbb{E}_{p \sim U[0,1]} \mathcal{L}(D, \hat{Q}, p)$ .

### 3.3 Encouraging calibration of centered intervals with the interval score

The calibration loss from 3.2 optimizes the average calibration of each quantile, i.e. the correct intended coverage below a quantile estimate. This can be considered optimizing for the correct coverage of a non-centered,  $p$  prediction interval (PI) between the levels  $[0, p]$ . In many applications, however, it is much more common to utilize a PI that is centered at the mean or median prediction. For an intended coverage of  $p$ , this would correspond to quantile estimates for the levels  $(0.5 - \frac{p}{2})$  and  $(0.5 + \frac{p}{2})$ .

To this end, we propose optimizing the **interval score**, which is a proper scoring rule for centered interval predictions (Gneiting and Raftery [2007]). For a given point  $(x, y)$ , denote a  $(1 - \alpha)$  centered PI as  $\hat{l}, \hat{u}$ , i.e.  $\hat{l} = \hat{Q}(x, \frac{\alpha}{2})$  and  $\hat{u} = \hat{Q}(x, 1 - \frac{\alpha}{2})$ . We omit conditioning on  $x$  for clarity. Then the interval score is defined as:

$$\begin{aligned} S_{\alpha}(\hat{l}, \hat{u}; y) = \\ (\hat{u} - \hat{l}) + \frac{2}{\alpha} (\hat{l} - y) \mathbb{I}\{y < \hat{l}\} + \frac{2}{\alpha} (y - \hat{u}) \mathbb{I}\{y > \hat{u}\}. \end{aligned}$$

This score presents an intuitive interpretation of the desirable components from a centered interval: the first term penalizes the width (sharpness), and the second and third terms penalize calibration (i.e. correct

coverage of PI) by penalizing the prediction when the datapoint falls outside the PI. For a higher intended coverage (i.e. lower  $\alpha$ ), the coverage penalty is scaled higher (scaled by  $\frac{2}{\alpha}$ ).

We can show that the minimum of the expectation of the interval score is attained at the true quantiles,  $\hat{l} = \mathbb{Q}(\cdot, \frac{\alpha}{2})$ ,  $\hat{u} = \mathbb{Q}(\cdot, 1 - \frac{\alpha}{2})$  (Appendix A.3), which motivates using empirical risk minimization to optimize the interval score. We train our quantile model for all centered intervals (and hence quantile levels) simultaneously by setting our loss objective as  $\mathbb{E}_{\alpha \sim U[0,1]} S_{\alpha}$ .

### 3.4 Inducing adversarial group calibration with group batching

The calibration loss from 3.2 and the interval score from 3.3 optimize for the *average* calibration of quantiles and centered intervals, respectively. To get closer to individual calibration, one condition we can additionally require is *adversarial group calibration*. Since adversarial group calibration requires average calibration over any subset of non-zero measure over the domain, this is not fully observable with finite datasets  $D$  for all subset sizes. However, for any subset in  $D$  with enough data, we can still estimate the subset’s average calibration. Hence, we can apply our optimization objectives onto appropriately large subsets to induce adversarial group calibration.

In practice, this involves constructing subsets within the domain and taking gradient steps based on the loss over each subset. In naive implementations of stochastic gradient descent, a random batch is drawn uniformly from the training dataset  $D$ , and a gradient step is taken according to the loss over this batch. This is also the case in SQR (Tagasovska and Lopez-Paz [2019]). The uniform draw of the batch will tend to preserve the marginal distribution over  $\mathcal{X}$ ,  $\mathbb{F}_{\mathbf{X}}$ , hence, optimizing average calibration over this batch will only induce average calibration of the model.

By deliberately grouping the datapoints based on input features and batching based on these groups, the distribution of each batch will not follow  $\mathbb{F}_{\mathbf{X}}$ , and taking optimization steps w.r.t. this group will induce better adversarial group calibration. We find in our experiments that adversarial group calibration improves significantly with simple implementations of group batching, and in Figure 1, we show that group batching can also improve calibration of SQR. Appendix C details how we implemented group batching.

## 4 Experiments

We demonstrate our proposed method’s performance on the standard 8 UCI datasets (Asuncion and Newman [2007]), and on a real-world problem in nuclear fusion. To assess the predictions, we use all metrics

from Section 2.2 that can be estimated with a finite test dataset: 1) average calibration vs sharpness, 2) adversarial group calibration, 3) interval calibration, 4) check score, and 5) interval score.

To measure the calibration metrics (average, interval, adversarial group), we scaled the expected probabilities from 0.01 to 0.99 in 0.01 increments and estimated ECE (4) according to this finite discretization. For interval calibration, for each expected probability  $p$ , we predict centered  $p$  PIs, and calculate  $\hat{p}_{avg}^{obs}$  as the proportion of test points falling within the PI. Appendix C details how we estimated adversarial group calibration. Sharpness was measured as the mean width of the 95% centered PI (i.e. between  $p = 0.025$  and  $0.975$ ). The proper scoring rules (check, interval) were measured as the average of the score on the test set.

We provide a comparison against current state-of-the-art UQ methods for which computing the above metrics is tractable. SQR (Tagasovska and Lopez-Paz [2019]) is an NN model that optimizes the pinball loss for a batch of random quantile levels  $p \sim U(0, 1)$ . Individual calibration (Zhao et al. [2020]) is a randomized extension of probabilistic neural networks (Lakshminarayanan et al. [2017], Nix and Weigend [1994]) that optimizes a combination of the standard Gaussian NLL and a loss that induces individual calibration.

While more quantile and PI based UQ methods exist, they are mostly designed to output a single quantile level or interval coverage level, which makes measuring calibration extremely expensive (training up to 100 models separately). For these methods, we provide a comparison on a simplified task of predicting 95% PI in Appendix B.3. Lastly, one method that can additionally be considered is the recalibration algorithm by Kuleshov et al. [2018]. This algorithm is not a standalone UQ method, but a refinement step that can be applied on top of other methods. We find that applying this recalibration may improve the average calibration of a prediction, but does so at a significant cost in sharpness, hence is not a robust remedy. We discuss recalibration results in Appendix B.4.

All experimental results report the mean and standard error across 5 trials: error bars and shades in plots indicate  $\pm 1$  standard error; in numeric tables, the mean is presented with 1 standard error in parentheses.

### 4.1 Benchmark UCI Datasets

We evaluate 5 methods on the 8 UCI datasets: three proposed algorithms—*MAQR*, *Cali* (penalized calibration loss), and *Interval* (interval score)—and 2 alternative algorithms—*SQR* and *IndvCal* (individual calibration). Results from the first 5 datasets in alphabetical order are presented, and the full set of results are

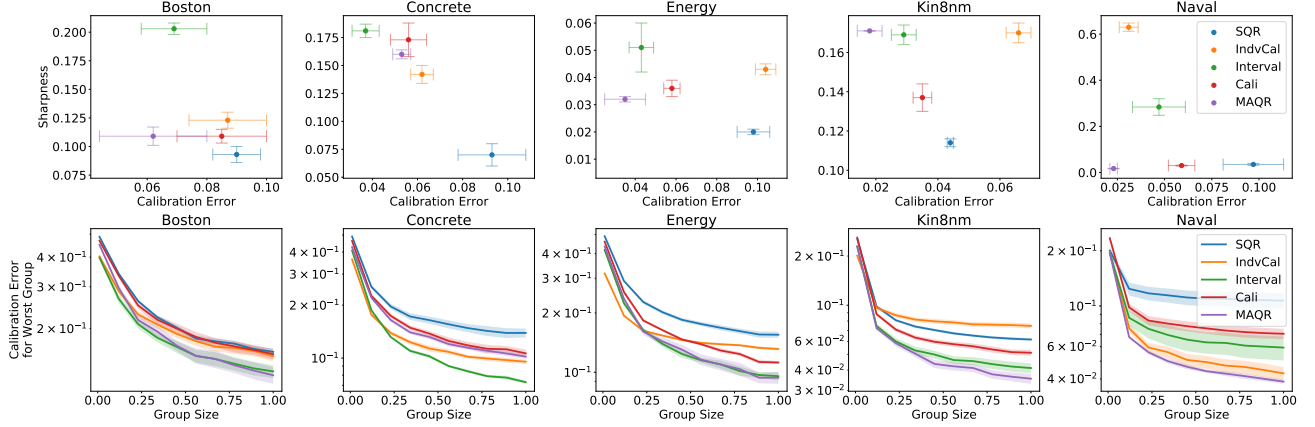


Figure 2: UCI Experiments. **Top row:** Average calibration and sharpness. **Bottom row:** Adversarial group calibration (group size refers to the proportion of dataset size). Full set of results (additional datasets) are in Appendix B.1.

	<i>SQR</i>	<i>MAQR</i>	<i>Interval</i>	<i>MAQR</i>	<i>Interval</i>	<i>MAQR</i>
Boston	0.088(0.008)	<b>0.063(0.016)</b>	1.010(0.118)	<b>0.864(0.287)</b>	<b>0.079(0.015)</b>	0.092(0.041)
Concrete	0.085(0.006)	<b>0.059(0.008)</b>	0.943(0.053)	<b>0.672(0.118)</b>	0.061(0.008)	<b>0.059(0.020)</b>
Energy	0.014(0.000)	<b>0.010(0.001)</b>	0.182(0.026)	<b>0.101(0.006)</b>	0.060(0.010)	<b>0.052(0.018)</b>
Kin8nm	0.078(0.001)	<b>0.070(0.001)</b>	0.776(0.017)	<b>0.691(0.015)</b>	0.048(0.006)	<b>0.019(0.008)</b>
Naval	0.070(0.001)	<b>0.004(0.000)</b>	0.620(0.114)	<b>0.044(0.001)</b>	0.043(0.014)	<b>0.012(0.002)</b>

Figure 3: UCI Experiments. **Left:** Check score. **Middle:** Interval score. **Right:** Interval Calibration. Each table shows the top two methods only, in terms of average performance. Full set of results (additional methods and datasets) are in Appendix B.1. The highest scoring results for each dataset are shown in **bold**.

in Appendix B.1. We use the the same NN architecture, learning rate, and training details for all methods. Appendix C.1 includes more details on the experiment setup and hyperparameters. The calibration-sharpness metrics are presented in the top row of Figure 2. *MAQR* achieves the best calibration on average across the datasets, and sometimes dominates other methods in *both* calibration and sharpness. Adversarial group calibration in the bottom row Figure 2 also indicates that *MAQR* tends to achieve lowest calibration error across *any* random group of *any* size with more than one point. The check and interval scores in the tables in Figure 3 also rank *MAQR*’s prediction as best, which is surprising given that *SQR* is a NN of the same capacity that was explicitly trained to optimize the check score, and likewise for *Interval* with the interval score. This indicates the distribution predicted by *MAQR* is fundamentally different as it utilizes direct estimates of the conditional distribution, while the other methods all optimize a specific loss function.

Excluding *MAQR*: The top row of Figure 2 shows *SQR*, *Interval* and *Cali* all producing competitive calibration-sharpness results (i.e. there is no other method that is dominant in *both* calibration and sharpness), with *IndvCal* performing the poorest. Notably,

*SQR* tends to produce the sharpest predictions, which is not surprising following Proposition 1. Adversarial group calibration (Figure 2, bottom row), however, suggests that *SQR*’s predictions have not approached the true conditional quantiles well: e.g. on the Energy dataset, *SQR* reports better average calibration (top row) on the full test set than *IndvCal*, but *IndvCal* is better adversarially calibrated than *SQR* (bottom row). Centered interval calibration in Appendix B.1 suggests that *Interval* produces better calibrated centered intervals, even when average calibration was worse (e.g. Power dataset, Appendix B.1).

## 4.2 Modeling Uncertainty in Nuclear Fusion

We further demonstrate the performance of our algorithms on a high-dimensional task from nuclear fusion: quantifying uncertainty in plasma dynamics. The plasma data was recorded from the DIII-D tokamak, a nuclear fusion device operated by General Atomics (Luxon [2002]). Plasma dynamics during fusion reactions are highly stochastic and running live fusion experiments is costly. Hence, practitioners use this dataset to learn a dynamics model of the system, for various purposes such as learning a controller to optimize reaction efficiency and stability (Fu et al. [2020], Boyer et al. [2019a,b]). There are 10 scalar tar-

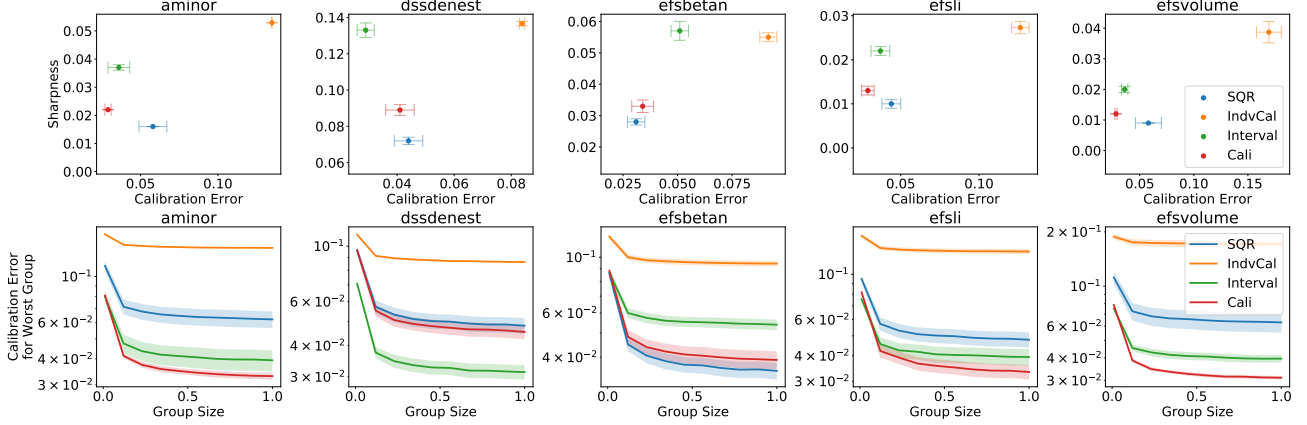


Figure 4: Nuclear Fusion Experiments. **Top row:** Average calibration and sharpness. **Bottom row:** Adversarial group calibration (group size refers to proportion of dataset size). Full set of results (additional signals) are in Appendix B.2.

	<i>SQR</i>	<i>IndvCal</i>	<i>Interval</i>	<i>Cali</i>
aminor	0.081(0.006)	0.268(0.000)	<b>0.055 (0.007)</b>	0.058(0.004)
dssdenest	0.072(0.003)	0.162(0.003)	<b>0.054 (0.006)</b>	0.071(0.008)
efsbetan	<b>0.051 (0.001)</b>	0.160(0.012)	0.087(0.009)	0.056(0.007)
efqli	0.071(0.011)	0.214(0.017)	0.069(0.013)	<b>0.043 (0.003)</b>
efsvolume	0.073(0.007)	0.315(0.022)	0.063(0.007)	<b>0.056 (0.002)</b>

Figure 5: Interval Calibration on Nuclear Fusion Experiments. The highest scoring results for each signal are shown in **bold**. Full set of results (additional signals and metrics) are in the Appendix B.2.

get signals to model in this dataset (full list in Appendix C.2), each describing a particular aspect of the current state of plasma. For each signal, the input features are 468 dimensional. We do not apply *MAQR* on this dataset because of the high computational costs and statistical challenge associated with nonparametric density estimation in high dimensions. Appendix C.2 provides more details on the data and experiment setup.

Results on the first 5 signals (alphabetical order) are presented here, and the full set of results are in Appendix B.2. The top row of Figure 4 shows a similar pattern across the signals: *SQR* produces the sharpest predictions, *Cali* and *Interval* are most calibrated with *Cali* sharper than *Interval*, and *IndvCal* performs the poorest with least calibrated and sharp predictions. It is generally known that plasma dynamics display complex stochasticity (Fu et al. [2020], Kowal et al. [2020]), and hence we suspect *IndvCal*’s performance degrades significantly because it assumes a Gaussian output and is trained according to the Gaussian likelihood.

Adversarial group calibration in bottom row of Figure 4 suggests that *SQR* has significantly traded off calibration for sharpness when compared to *Cali* and *Interval*. Comparing *Cali* and *Interval*, we see that *Cali* oftentimes dominates *Interval* in both average

calibration and sharpness, and also achieves better adversarial group calibration. Interval calibration in the table in Figure 5 also shows that *Cali* produces competitive centered intervals, suggesting that *Cali* has better estimated the conditional quantiles, in general.

## 5 Discussion

In this paper, we proposed four methods to improve quantile estimates for calibrated uncertainty quantification in regression. We assert that the pinball loss does not directly target key properties of interest (e.g. calibration, sharpness), and that our proposed methods provide more adequate means of producing uncertainty estimates with these properties. We have also extended the scope of regression models on which quantile-based UQ can be applied by developing a model-agnostic method. This can be of practical interest to users that have specific training infrastructure or preexisting regression methods since these methods can be leveraged to quantify uncertainty without additional overhead.

In certain applications, users may also be concerned with modeling epistemic uncertainty. This is somewhat orthogonal to the goals of this paper; nevertheless, we provide a discussion on how bootstrapped ensembles of our methods can incorporate epistemic uncertainty in Appendix D.



## References

- Bobak Shahriari, Kevin Swersky, Ziyu Wang, Ryan P Adams, and Nando De Freitas. Taking the human out of the loop: A review of bayesian optimization. *Proceedings of the IEEE*, 104(1):148–175, 2015.
- Jonas Mockus, Vytautas Tiesis, and Antanas Zilinskas. The application of bayesian methods for seeking the extremum. *Towards global optimization*, 2(117-129):2, 1978.
- Tianhe Yu, Garrett Thomas, Lantao Yu, Stefano Ermon, James Zou, Sergey Levine, Chelsea Finn, and Tengyu Ma. Mopo: Model-based offline policy optimization. *arXiv preprint arXiv:2005.13239*, 2020.
- Ali Malik, Volodymyr Kuleshov, Jiaming Song, Danny Nemer, Harlan Seymour, and Stefano Ermon. Calibrated model-based deep reinforcement learning. *arXiv preprint arXiv:1906.08312*, 2019.
- Kurtland Chua, Roberto Calandra, Rowan McAllister, and Sergey Levine. Deep reinforcement learning in a handful of trials using probabilistic dynamics models. In *Advances in Neural Information Processing Systems*, pages 4754–4765, 2018.
- Javier Garcia and Fernando Fernández. Safe exploration of state and action spaces in reinforcement learning. *Journal of Artificial Intelligence Research*, 45:515–564, 2012.
- Cynthia Rudin. Stop explaining black box machine learning models for high stakes decisions and use interpretable models instead. *Nature Machine Intelligence*, 1(5):206–215, 2019.
- Rebecca Wexler. When a computer program keeps you in jail: How computers are harming criminal justice. *New York Times*, 13, 2017.
- Shengjia Zhao, Tengyu Ma, and Stefano Ermon. Individual calibration with randomized forecasting. *arXiv preprint arXiv:2006.10288*, 2020.
- Nicki S Detlefsen, Martin Jørgensen, and Søren Hauberg. Reliable training and estimation of variance networks. *arXiv preprint arXiv:1906.03260*, 2019.
- Balaji Lakshminarayanan, Alexander Pritzel, and Charles Blundell. Simple and scalable predictive uncertainty estimation using deep ensembles. In *Advances in neural information processing systems*, pages 6402–6413, 2017.
- Wesley J Maddox, Pavel Izmailov, Timur Garipov, Dmitry P Vetrov, and Andrew Gordon Wilson. A simple baseline for bayesian uncertainty in deep learning. In *Advances in Neural Information Processing Systems*, pages 13153–13164, 2019.
- Jeremiah Liu, John Paisley, Marianthi-Anna Kioumourtzoglou, and Brent Coull. Accurate uncertainty estimation and decomposition in ensemble learning. In *Advances in Neural Information Processing Systems*, pages 8950–8961, 2019.
- José Miguel Hernández-Lobato and Ryan Adams. Probabilistic backpropagation for scalable learning of bayesian neural networks. In *International Conference on Machine Learning*, pages 1861–1869, 2015.
- Charles Blundell, Julien Cornebise, Koray Kavukcuoglu, and Daan Wierstra. Weight uncertainty in neural networks. *arXiv preprint arXiv:1505.05424*, 2015.
- Daphne Koller and Nir Friedman. *Probabilistic graphical models: principles and techniques*. MIT press, 2009.
- Carl Edward Rasmussen. Gaussian processes in machine learning. In *Summer School on Machine Learning*, pages 63–71. Springer, 2003.
- Tárik S Salem, Helge Langseth, and Heri Ramampiaro. Prediction intervals: Split normal mixture from quality-driven deep ensembles. In *Conference on Uncertainty in Artificial Intelligence*, pages 1179–1187. PMLR, 2020.
- Natasa Tagasovska and David Lopez-Paz. Single-model uncertainties for deep learning. In *Advances in Neural Information Processing Systems*, pages 6414–6425, 2019.
- Tim Pearce, Mohamed Zaki, Alexandra Brintrup, and Andy Neely. High-quality prediction intervals for deep learning: A distribution-free, ensembled approach. *arXiv preprint arXiv:1802.07167*, 2018a.
- Lingxin Hao, Daniel Q Naiman, and Daniel Q Naiman. *Quantile regression*. Number 149. Sage, 2007.
- Roger Koenker and Kevin F Hallock. Quantile regression. *Journal of economic perspectives*, 15(4):143–156, 2001.
- Koenker. *Quantile Regression (Econometric Society Monographs; No. 38)*. Cambridge university press, 2005.
- Filipe Rodrigues and Francisco C Pereira. Beyond expectation: deep joint mean and quantile regression for spatiotemporal problems. *IEEE Transactions on Neural Networks and Learning Systems*, 2020.
- Kevin Tran, Willie Neiswanger, Junwoong Yoon, Qingyang Zhang, Eric Xing, and Zachary W Ulissi. Methods for comparing uncertainty quantifications for material property predictions. *Machine Learning: Science and Technology*, 1(2):025006, 2020.
- Volodymyr Kuleshov, Nathan Fenner, and Stefano Ermon. Accurate uncertainties for deep learning using calibrated regression. *arXiv preprint arXiv:1807.00263*, 2018.

- Chuan Guo, Geoff Pleiss, Yu Sun, and Kilian Q Weinberger. On calibration of modern neural networks. In *Proceedings of the 34th International Conference on Machine Learning-Volume 70*, pages 1321–1330. JMLR. org, 2017.
- Tilman Gneiting, Fadoua Balabdaoui, and Adrian E Raftery. Probabilistic forecasts, calibration and sharpness. *Journal of the Royal Statistical Society: Series B (Statistical Methodology)*, 69(2):243–268, 2007.
- Allan H Murphy. A new vector partition of the probability score. *Journal of applied Meteorology*, 12(4): 595–600, 1973.
- Ursula Hébert-Johnson, Michael P Kim, Omer Rein-gold, and Guy N Rothblum. Calibration for the (computationally-identifiable) masses. *arXiv preprint arXiv:1711.08513*, 2017.
- Jon Kleinberg, Sendhil Mullainathan, and Manish Raghavan. Inherent trade-offs in the fair determination of risk scores. *arXiv preprint arXiv:1609.05807*, 2016.
- Tilman Gneiting and Adrian E Raftery. Strictly proper scoring rules, prediction, and estimation. *Journal of the American statistical Association*, 102 (477):359–378, 2007.
- Tim Pearce, Felix Leibfried, Alexandra Brintrup, Mohamed Zaki, and Andy Neely. Uncertainty in neural networks: Approximately bayesian ensembling. *arXiv preprint arXiv:1810.05546*, 2018b.
- Roger Koenker and Gilbert Bassett Jr. Regression quantiles. *Econometrica: journal of the Econometric Society*, pages 33–50, 1978.
- Alex J Cannon. Non-crossing nonlinear regression quantiles by monotone composite quantile regression neural network, with application to rainfall extremes. *Stochastic environmental research and risk assessment*, 32(11):3207–3225, 2018.
- Qifa Xu, Kai Deng, Cuixia Jiang, Fang Sun, and Xue Huang. Composite quantile regression neural network with applications. *Expert Systems with Applications*, 76:129–139, 2017.
- Yarin Gal and Zoubin Ghahramani. Dropout as a bayesian approximation: Representing model uncertainty in deep learning. In *international conference on machine learning*, pages 1050–1059, 2016.
- Michael P Holmes, Alexander G Gray, and Charles Lee Isbell. Fast nonparametric conditional density estimation. *arXiv preprint arXiv:1206.5278*, 2012.
- Rob J Hyndman, David M Bashtannyk, and Gary K Grunwald. Estimating and visualizing conditional densities. *Journal of Computational and Graphical Statistics*, 5(4):315–336, 1996.
- Winfried Stute et al. On almost sure convergence of conditional empirical distribution functions. *The Annals of Probability*, 14(3):891–901, 1986.
- Arthur Asuncion and David Newman. Uci machine learning repository, 2007.
- David A Nix and Andreas S Weigend. Estimating the mean and variance of the target probability distribution. In *Proceedings of 1994 ieee international conference on neural networks (ICNN’94)*, volume 1, pages 55–60. IEEE, 1994.
- James L Luxon. A design retrospective of the diii-d tokamak. *Nuclear Fusion*, 42(5):614, 2002.
- Yichen Fu, David Eldon, Keith Erickson, Kornee Kleijwegt, Leonard Lupin-Jimenez, Mark D Boyer, Nick Eidiotis, Nathaniel Barbour, Olivier Izacard, and Egemen Kolemen. Machine learning control for disruption and tearing mode avoidance. *Physics of Plasmas*, 27(2):022501, 2020.
- MD Boyer, KG Erickson, BA Grierson, DC Pace, JT Scoville, J Rauch, BJ Crowley, JR Ferron, SR Haskey, DA Humphreys, et al. Feedback control of stored energy and rotation with variable beam energy and perveance on diii-d. *Nuclear Fusion*, 59 (7):076004, 2019a.
- MD Boyer, S Kaye, and K Erickson. Real-time capable modeling of neutral beam injection on nstx-u using neural networks. *Nuclear Fusion*, 59(5):056008, 2019b.
- Grzegorz Kowal, Diego A Falceta-Gonçalves, Alex Lazarian, and Ethan T Vishniac. Kelvin–helmholtz versus tearing instability: What drives turbulence in stochastic reconnection? *The Astrophysical Journal*, 892(1):50, 2020.
- Nicolai Meinshausen. Quantile regression forests. *Journal of Machine Learning Research*, 7(Jun):983–999, 2006.

## Appendix

---

### A Theoretical Results

#### A.1 Proof of Proposition 1

**Proposition 1** Consider a dataset  $D = \{(x_i, y_i)\}_{i=1}^N$  with unique  $x_i \in \mathcal{X}$ , model class  $F$  with an infinite capacity, and pinball loss  $\rho_\tau(y, \hat{y}) = (\hat{y} - y)(\mathbb{I}\{y \leq \hat{y}\} - \tau)$ . For any level  $\tau \in [0, 1]$ , the minimizer  $\arg\min_{f \in F} \left[ \sum_{i=1}^N \rho_\tau(y_i, f(x_i)) \right]$  achieves 0 pinball loss. However, these minimizers yield a miscalibrated uncertainty prediction with  $ECE = 0.5$ .

**Proof**

For any given  $\tau \in [0, 1]$ , denote by  $L_\tau$  the sum of the pinball loss terms for each datapoint in the dataset  $D$ , i.e.

$$\begin{aligned} L_\tau &= \sum_{i=1}^N \rho_\tau(y_i, f(x_i)) \\ &= \sum_{i=1}^N (f(x_i) - y_i)(\mathbb{I}\{y_i \leq f(x_i)\} - \tau) \end{aligned}$$

Denote  $l_i = (f(x_i) - y_i)(\mathbb{I}\{y_i \leq f(x_i)\} - \tau)$ .

Case (A): When  $\tau \in (0, 1)$ ,

- If  $y_i < f(x_i)$ :  $l_i = (f(x_i) - y_i)(1 - \tau)$ .  
Here,  $f(x_i) - y_i > 0$ ,  $1 - \tau > 0$ .
- If  $y_i > f(x_i)$ :  $l_i = (f(x_i) - y_i)(-\tau) = (y_i - f(x_i))\tau$ .  
Here,  $y_i - f(x_i) > 0$ ,  $\tau > 0$ .
- If  $y_i = f(x_i)$ :  $l_i = 0$ .

Therefore, for any  $\tau \in (0, 1)$ ,  $l_i$  is minimized when  $y_i = f(x_i)$ , which is when  $\hat{p}_{avg}^{\text{obs}}(p) = 1$ .

Case (B): When  $\tau = 0$ ,

- If  $y_i < f(x_i)$ :  $l_i = f(x_i) - y_i > 0$ .
- If  $y_i > f(x_i)$ :  $l_i = (f(x_i) - y_i)(-\tau) = 0$ , which is when  $\hat{p}_{avg}^{\text{obs}}(p) = 0$ .
- If  $y_i = f(x_i)$ :  $l_i = 0$ , which is when  $\hat{p}_{avg}^{\text{obs}}(p) = 1$ .

Case (C): When  $\tau = 1$ ,

- If  $y_i < f(x_i)$ :  $l_i = (f(x_i) - y_i)(1 - \tau) = 0$ , which is when  $\hat{p}_{avg}^{\text{obs}}(p) = 1$ .
- If  $y_i > f(x_i)$ :  $l_i = (f(x_i) - y_i)(-\tau) = (y_i - f(x_i))(\tau) > 0$ .
- If  $y_i = f(x_i)$ :  $l_i = 0$ , which is when  $\hat{p}_{avg}^{\text{obs}}(p) = 1$ .

By cases (A), (B), (C), we can see that there are 2 ways for the minimum of  $L_\tau$  to be attained:

- (i)  $\hat{p}_{avg}^{\text{obs}}(p) = 1$  for all  $\tau \in [0, 1]$ .
- (ii)  $\hat{p}_{avg}^{\text{obs}}(p) = 1$  for all  $\tau \in (0, 1]$  and  $\hat{p}_{avg}^{\text{obs}}(p) = 0$  for  $\tau = 0$ .

Suppose we use  $T$  equispaced discretizations of  $\tau \in [0, 1]$  to estimate ECE (Equation 4).

- In the first minima case (i) when  $\hat{p}_{avg}^{\text{obs}}(p) = 1$  for all  $\tau \in [0, 1]$ ,  
 $\widehat{\text{ECE}} = \frac{1}{T} \sum_{\tau \in [0, 1]} (1 - \tau) = \frac{1}{T} (T - \frac{T}{2}) = 0.5$
- In the second minima case (ii) when  $\hat{p}_{avg}^{\text{obs}}(p) = 1$  for all  $\tau \in (0, 1]$  and  $\hat{p}_{avg}^{\text{obs}}(p) = 0$  for  $\tau = 0$ ,  
 $\widehat{\text{ECE}} = (\frac{1}{T} \times 0) + \frac{1}{T} \sum_{\tau \in (0, 1]} (1 - \tau) = \frac{1}{T} (T - \frac{(T-1)(1+\epsilon)}{2})$  where  $\epsilon$  is the first non-zero value of  $\tau$ . Then  
 $\frac{1}{T} (T - \frac{(T-1)(1+\epsilon)}{2}) = 1 - \frac{(1-\frac{1}{T})(1+\epsilon)}{2}$   
 $1 - \frac{(1-\frac{1}{T})(1+\epsilon)}{2} \rightarrow 0.5$  as  $T \rightarrow \infty$  (because  $\epsilon \rightarrow 0$  as  $T \rightarrow \infty$ ).  $\square$

## A.2 Model Agnostic Quantile Regression

As stated in Section 3.1, Algorithm 1 is one implementation of a general model-agnostic quantile regression procedure, in which we take direct estimates of the target density and regress onto these estimates. This general framework is state in Algorithm 2

---

### Algorithm 2 General Algorithm for Model Agnostic Quantile Regression

---

- 1: **Input:** Train data  $\{x_i, y_i\}_{i=1}^N$
  - 2: Initialize  $D \leftarrow \emptyset$
  - 3: **for**  $i = 1$  **to**  $N$  **do**
  - 4:   Select a set of quantile levels  $\{p_k\}_{k=1}^m$ ,  $p_k \in [0, 1]$
  - 5:    $\hat{q}_{i,p_k} \leftarrow$  KDE estimate of  $\mathbb{Q}(x_i, p_k)$ ,  $k = 1, \dots, m$
  - 6:    $D \leftarrow D \cup \{x_i, p_k, \hat{q}_{i,p_k}\}_{k=1}^m$
  - 7: **end for**
  - 8: Use  $D$  to fit a regression model  $\hat{\mathbb{Q}}$   
 $\hat{\mathbb{Q}} : (x_i, p_k) \mapsto \hat{q}_{i,p_k}$ ,  $k = 1, \dots, m$
  - 9: **Output:**  $\hat{q}$ ,  $k = 1, \dots, m$
- 

Algorithm 1 implements the KDE step of Algorithm 2 (line 5 of Algorithm 2) by using a uniform kernel over  $\mathcal{X}$  (line 5 of Algorithm 1) and  $\mathcal{Y}$  (lines 6, 7, 8 of Algorithm 1). In this case, the quantile estimates  $\{p_k, \hat{q}_{i,p_k}\}$  is exactly the estimator  $\{m_n(\hat{q}_{i,p_k} | x_i), \hat{q}_{i,p_k}\}$  from Stute et al. [1986], and under mild assumptions on the bandwidth of the kernel over  $\mathcal{X}$ , by Theorem 1 of Stute et al. [1986], the quantile dataset  $D$  in line 9 of Algorithm 1 is consistent for almost all  $x \in \mathcal{X}$ , i.e. for almost all  $x \in \mathcal{X}$ , the conditional quantile estimates approach the true conditional quantiles almost surely as the number of datapoints  $N \rightarrow \infty$ . We refer the reader to Stute et al. [1986] for details on the proof. What this signifies is that in the limit of datapoints, the regression targets for the quantile model will be the true conditional quantiles, and hence, the labels we attribute to each quantile and quantile level are in fact the true underlying values.

It should also be noted that many other conditional KDE methods can be used to construct the dataset  $D$ . We refer the reader to Holmes et al. [2012], Hyndman et al. [1996] for a more thorough treatment of methods in conditional KDE.

## A.3 Optimum of Interval Score

Following notation from Section 3.3, we denote  $\hat{l} = \hat{\mathbb{Q}}(x, \frac{\alpha}{2})$  and  $\hat{u} = \hat{\mathbb{Q}}(x, 1 - \frac{\alpha}{2})$ , and we omit conditioning on  $x$  for clarity.



Assume  $\hat{l} \leq \hat{u}$ . Then,

$$\begin{aligned}
 & \mathbb{E} [S_\alpha(\hat{l}, \hat{u}; y)] \\
 &= \int_{-\infty}^{\hat{l}} S_\alpha(\hat{l}, \hat{u}; y) d\mathbb{F}(y) + \int_{\hat{l}}^{\hat{u}} S_\alpha(\hat{l}, \hat{u}; y) d\mathbb{F}(y) + \int_{\hat{u}}^{\infty} S_\alpha(\hat{l}, \hat{u}; y) d\mathbb{F}(y) \\
 &= (\hat{u} - \hat{l}) + \frac{2}{\alpha} \int_{-\infty}^{\hat{l}} (\hat{l} - y) d\mathbb{F}(y) + \frac{2}{\alpha} \int_{\hat{u}}^{\infty} (y - \hat{u}) d\mathbb{F}(y) \\
 & \frac{\partial \mathbb{E} [S_\alpha(\hat{l}, \hat{u}; y)]}{\partial \hat{l}} = -1 + \frac{2}{\alpha} \int_{-\infty}^{\hat{l}} d\mathbb{F}(y) = -1 + \frac{2}{\alpha} \mathbb{F}(\hat{l}) \\
 & \frac{\partial \mathbb{E} [S_\alpha(\hat{l}, \hat{u}; y)]}{\partial \hat{u}} = 1 - \frac{2}{\alpha} \int_{\hat{u}}^{\infty} d\mathbb{F}(y) = 1 - \frac{2}{\alpha} (1 - \mathbb{F}(\hat{u})).
 \end{aligned}$$

Setting  $\frac{\partial \mathbb{E} [S_\alpha(\hat{l}, \hat{u}; y)]}{\partial \hat{l}}$  and  $\frac{\partial \mathbb{E} [S_\alpha(\hat{l}, \hat{u}; y)]}{\partial \hat{u}}$  to zero reveals the interval loss minima at the respective true quantiles  $\mathbb{F}(\hat{l}) = \frac{\alpha}{2}$ ,  $\mathbb{F}(\hat{u}) = 1 - \frac{\alpha}{2}$ , i.e.  $\hat{l} = \mathbb{Q}(\cdot, \frac{\alpha}{2})$ ,  $\hat{u} = \mathbb{Q}(\cdot, 1 - \frac{\alpha}{2})$ .  $\square$

## B Full Experimental Results

### B.1 Full UCI Experiment Results

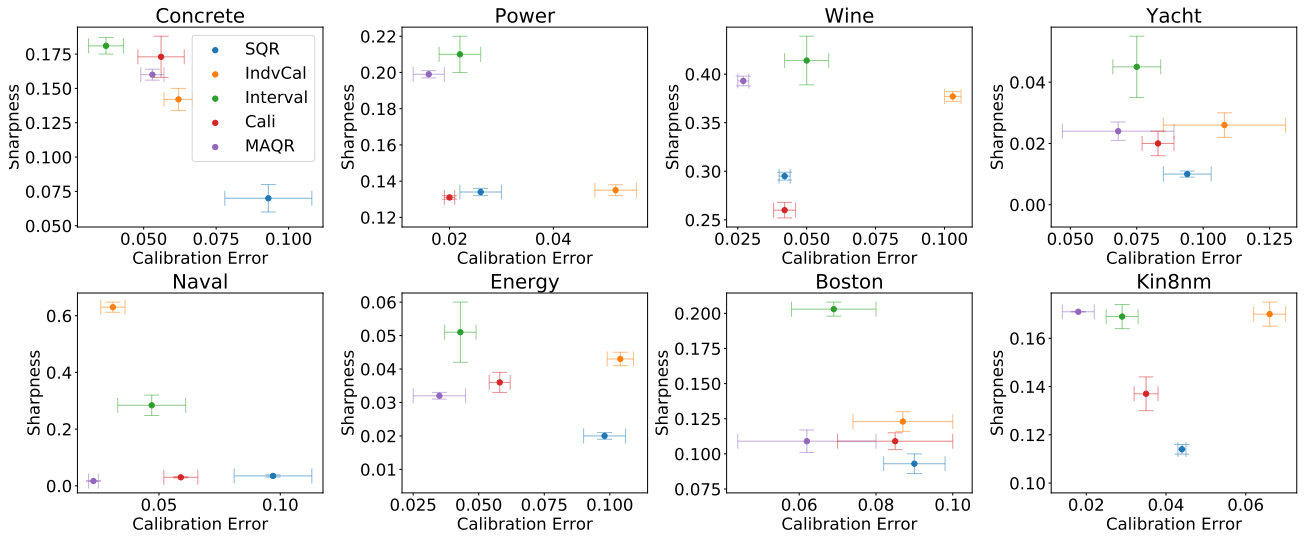
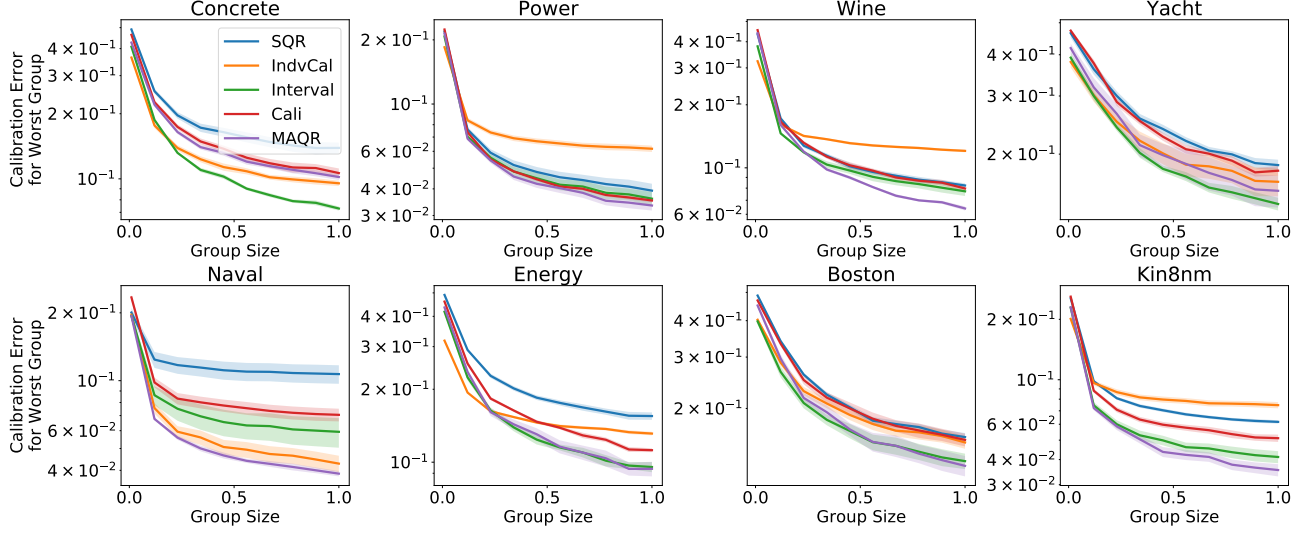


Figure 6: UCI Average Calibration-Sharpness. Full results of Section 4.1, Figure 2, Top Row


 Figure 7: **UCI Adversarial Group Calibration.** Full results of Section 4.1, Figure 2, Bottom Row

	<i>SQR</i>	<i>IndvCal</i>	<i>Interval</i>	<i>Cali</i>	<i>MAQR</i>
concrete	0.085(0.006)	0.085(0.005)	0.086(0.004)	0.118(0.006)	<b>0.059 (0.008)</b>
power	<b>0.057(0.001)</b>	0.070(0.001)	0.062(0.001)	0.064(0.001)	0.058(0.001)
wine	0.205(0.008)	0.219(0.004)	0.214(0.006)	0.210(0.008)	<b>0.191 (0.003)</b>
yacht	0.012(0.002)	0.015(0.002)	0.018(0.003)	0.019(0.004)	<b>0.007 (0.001)</b>
naval	0.070(0.001)	0.276(0.004)	0.066(0.013)	0.159(0.029)	<b>0.004 (0.000)</b>
energy	0.014(0.000)	0.015(0.001)	0.017(0.003)	0.017(0.002)	<b>0.010 (0.001)</b>
boston	0.088(0.008)	0.095(0.008)	0.094(0.009)	0.103(0.013)	<b>0.063 (0.016)</b>
kin8nm	0.078(0.001)	0.104(0.003)	0.077(0.001)	0.096(0.005)	<b>0.070 (0.001)</b>

 Figure 8: **UCI Check Score.** Full check score results of Section 4.1, Figure 3, Left Table.

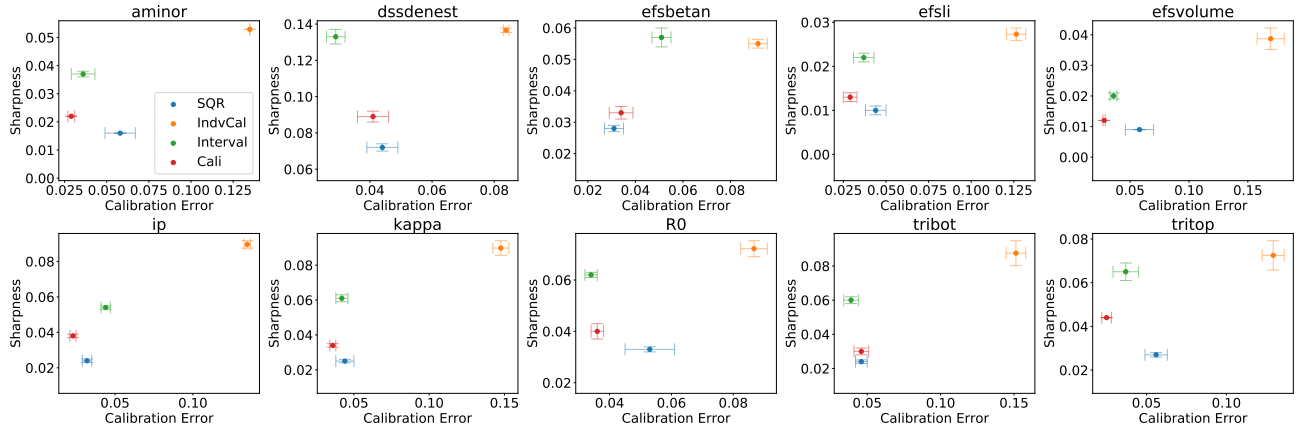
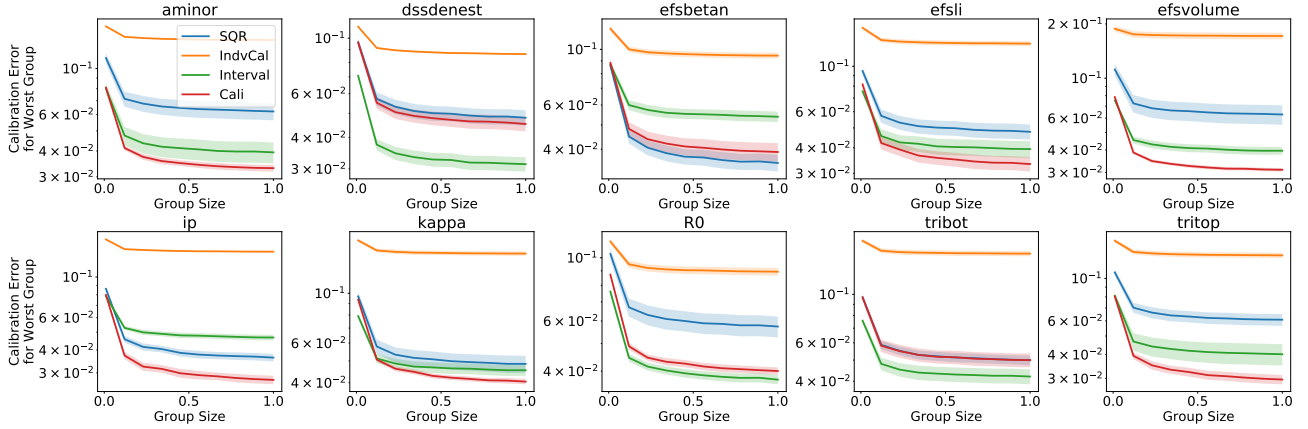
	<i>SQR</i>	<i>IndvCal</i>	<i>Interval</i>	<i>Cali</i>	<i>MAQR</i>
concrete	2.038(0.225)	1.157(0.069)	0.943(0.053)	1.465(0.086)	<b>0.672 (0.118)</b>
power	0.834(0.022)	0.917(0.021)	0.620(0.010)	0.699(0.019)	<b>0.592 (0.009)</b>
wine	3.242(0.166)	3.168(0.019)	2.197(0.045)	2.498(0.135)	<b>2.052 (0.052)</b>
yacht	0.314(0.061)	0.197(0.036)	0.190(0.021)	0.298(0.063)	<b>0.086 (0.016)</b>
naval	0.097(0.011)	3.112(0.053)	0.620(0.114)	1.560(0.268)	<b>0.044 (0.001)</b>
energy	0.290(0.016)	0.223(0.017)	0.182(0.026)	0.204(0.018)	<b>0.101 (0.006)</b>
boston	1.833(0.299)	1.395(0.176)	1.010(0.118)	1.449(0.259)	<b>0.864 (0.287)</b>
kin8nm	1.241(0.041)	1.347(0.031)	0.776(0.017)	1.121(0.072)	<b>0.691 (0.015)</b>

 Figure 9: **UCI Interval Score** Full interval score results of Section 4.1, Figure 3, Middle Table.

	<i>SQR</i>	<i>IndvCal</i>	<i>Interval</i>	<i>Cali</i>	<i>MAQR</i>
concrete	0.186(0.031)	0.089(0.005)	0.061(0.008)	0.096(0.013)	<b>0.059 (0.020)</b>
power	0.045(0.004)	0.068(0.008)	0.023(0.003)	0.037(0.002)	<b>0.010 (0.002)</b>
wine	0.053(0.006)	0.169(0.008)	0.079(0.014)	0.065(0.007)	<b>0.045 (0.005)</b>
yacht	0.135(0.009)	0.100(0.020)	0.121(0.005)	0.129(0.016)	<b>0.085 (0.024)</b>
naval	0.128(0.031)	0.039(0.003)	0.043(0.014)	0.110(0.013)	<b>0.012 (0.002)</b>
energy	0.174(0.011)	0.163(0.009)	0.060(0.010)	0.090(0.011)	<b>0.052 (0.018)</b>
boston	0.163(0.020)	<b>0.050 (0.007)</b>	0.079(0.015)	0.138(0.028)	0.092(0.041)
kin8nm	0.070(0.005)	0.080(0.002)	0.048(0.006)	0.067(0.005)	<b>0.019 (0.008)</b>

 Figure 10: **UCI Interval Calibration** Full interval calibration results of Section 4.1, Figure 3, Right Table.

## B.2 Full Fusion Experiment Results


 Figure 11: **Fusion Average Calibration-Sharpness** Full results of Section 4.2, Figure 4, Top Row.

 Figure 12: **Fusion Adversarial Group Calibration** Full results of Section 4.2, Figure 4, Bottom Row.

	<i>SQR</i>	<i>IndvCal</i>	<i>Interval</i>	<i>Cali</i>
aminor	<b>0.087 (0.000)</b>	0.182(0.000)	0.097(0.002)	0.092(0.002)
dssdenest	<b>0.179 (0.003)</b>	0.273(0.003)	0.180(0.001)	0.184(0.002)
betan	<b>0.146 (0.001)</b>	0.253(0.005)	0.153(0.002)	0.150(0.001)
li	<b>0.097 (0.001)</b>	0.166(0.003)	0.102(0.001)	0.104(0.001)
volume	<b>0.051 (0.001)</b>	0.107(0.007)	0.053(0.001)	0.052(0.001)
ip	<b>0.068 (0.000)</b>	0.199(0.011)	0.077(0.002)	0.076(0.001)
kappa	<b>0.072 (0.001)</b>	0.150(0.004)	0.079(0.002)	0.078(0.001)
R0	<b>0.120 (0.001)</b>	0.208(0.002)	0.126(0.002)	0.130(0.005)
tribot	<b>0.084 (0.001)</b>	0.184(0.020)	0.092(0.001)	0.096(0.005)
tritop	<b>0.102 (0.001)</b>	0.200(0.018)	0.107(0.004)	0.107(0.002)

 Figure 13: **Fusion Check Score** Full check score results of fusion experiment of Section 4.2

	<i>SQR</i>	<i>IndvCal</i>	<i>Interval</i>	<i>Cali</i>
aminor	1.181(0.007)	3.225(0.000)	<b>1.090 (0.017)</b>	1.207(0.035)
dssdenest	2.387(0.060)	4.352(0.109)	<b>1.995 (0.011)</b>	2.369(0.054)
betan	1.970(0.013)	4.301(0.124)	<b>1.725 (0.021)</b>	2.002(0.046)
li	1.354(0.018)	2.923(0.088)	<b>1.146 (0.010)</b>	1.410(0.015)
volume	0.711(0.023)	2.036(0.154)	<b>0.602 (0.012)</b>	0.697(0.026)
ip	0.906(0.005)	3.203(0.295)	<b>0.845 (0.017)</b>	0.978(0.026)
kappa	1.010(0.010)	2.639(0.101)	<b>0.891 (0.015)</b>	1.066(0.020)
R0	1.599(0.011)	3.310(0.064)	<b>1.414 (0.012)</b>	1.709(0.057)
tribot	1.211(0.009)	3.185(0.242)	<b>1.074 (0.012)</b>	1.421(0.115)
tritop	1.481(0.022)	3.564(0.351)	<b>1.232 (0.034)</b>	1.444(0.031)

 Figure 14: **Fusion Interval Score** Full interval score results of fusion experiment of Section 4.2

	<i>SQR</i>	<i>IndvCal</i>	<i>Interval</i>	<i>Cali</i>
aminor	0.081(0.006)	0.268(0.000)	<b>0.055 (0.007)</b>	0.058(0.004)
dssdenest	0.072(0.003)	0.162(0.003)	<b>0.054 (0.006)</b>	0.071(0.008)
betan	<b>0.051 (0.001)</b>	0.160(0.012)	0.087(0.009)	0.056(0.007)
li	0.071(0.011)	0.214(0.017)	0.069(0.013)	<b>0.043 (0.003)</b>
volume	0.073(0.007)	0.315(0.022)	0.063(0.007)	<b>0.056 (0.002)</b>
ip	0.051(0.003)	0.227(0.020)	0.077(0.015)	<b>0.036 (0.003)</b>
kappa	0.069(0.008)	0.254(0.014)	0.078(0.011)	<b>0.053 (0.004)</b>
R0	0.068(0.007)	0.168(0.009)	<b>0.058 (0.007)</b>	0.066(0.004)
tribot	0.087(0.006)	0.227(0.016)	<b>0.074 (0.008)</b>	0.080(0.007)
tritop	0.077(0.006)	0.231(0.017)	0.058(0.015)	<b>0.037 (0.004)</b>

 Figure 15: **Fusion Interval Calibration** Full interval calibration results experiments of Section 4.2, Figure 5

### B.3 Comparison on 95% Prediction Interval Task

In Section 4.1, we have presented an experiment that is targeted at evaluating the *full predictive distribution* on the 8 UCI datasets.

In this section, we present an experiment that is targeted at constructing a 95% *centered prediction interval (PI)* on the same UCI datasets, for the purposes of comparing against other quantile-based algorithms that are designed to output only a single quantile level. This experiment setup is exactly the same as the prediction intervals experiments in Section 4.1 of the work by Tagasovska and Lopez-Paz [2019], and we follow the exact same experiment procedure for a direct comparison against their reported results.

The comparison algorithms here are:



- Dropout (Gal and Ghahramani [2016]): a NN that uses a dropout layer during testing for multiple predictions
- QualityDriven (Pearce et al. [2018a]): a NN that optimizes a Binomial likelihood approximation as a surrogate loss for calibration and sharpness
- GradientBoosting (Meinshausen [2006]): a decision tree based model that optimizes the pinball loss with gradient boosting
- QuantileForest (Meinshausen [2006]): a decision tree based model that predicts the quantiles based on the trained output of a random forest
- ConditionalGaussian (Lakshminarayanan et al. [2017]): a probabilistic NN that optimizes the Gaussian NLL to output the parameters of a Gaussian distribution

We show the performance of MAQR to represent our proposed methods in this experiment, since MAQR performs the best on the full predictive distribution evaluations in Section 4.1. We also omit the results of SQR (Tagasovska and Lopez-Paz [2019]) in this experiment since we perform a full evaluation comparison with SQR in Section 4.1, and the purpose here is to compare our proposed method against the additional baselines.

In this experiment, since we only output two quantile levels (0.025, 0.975) to construct a single 95% prediction interval, we do not assess calibration (which requires the predictions for all quantile levels) and assess only the observed proportion of test points within the PI (also referred to as “prediction interval coverage probability” or “PICP”) and sharpness represented by the width of the PI (also referred to as “mean prediction interval width” or “MPIW”). We refer the reader to Tagasovska and Lopez-Paz [2019] for exact details on the experiment setup and the hyperparameters tuned. For MAQR, we used the exact same NN architecture (1 layer of 64 hidden units, ReLU non-linearities) as the NN based baselines (Dropout, QualityDriven, ConditionalGaussian) and the same training procedure as detailed in Tagasovska and Lopez-Paz [2019]. The hyperparameters tuned for MAQR are detailed in Appendix C.1.

	<i>Dropout</i>	<i>QualityDriven</i>	<i>GradientBoostingQR</i>
concrete	none	none	$0.93 \pm 0.00$ ( $0.71 \pm 0.00$ )
power	$0.94 \pm 0.00$ ( $0.37 \pm 0.00$ )	$0.93 \pm 0.02$ ( $0.34 \pm 0.19$ )	none
wine	none	none	none
yacht	$0.97 \pm 0.03$ ( $0.10 \pm 0.01$ )	$0.92 \pm 0.05$ ( $0.04 \pm 0.01$ )	$0.95 \pm 0.02$ ( $0.79 \pm 0.01$ )
naval	$0.96 \pm 0.01$ ( $0.23 \pm 0.00$ )	$0.94 \pm 0.02$ ( $0.21 \pm 0.11$ )	none
energy	$0.91 \pm 0.04$ ( $0.17 \pm 0.01$ )	$0.91 \pm 0.04$ ( $0.10 \pm 0.05$ )	none
boston	none	none	$0.89 \pm 0.00$ ( $0.75 \pm 0.00$ )
kin8nm	none	$0.96 \pm 0.00$ ( $0.84 \pm 0.00$ )	none
	<i>QuantileForest</i>	<i>ConditionalGaussian</i>	<i>MAQR</i>
concrete	$0.96 \pm 0.01$ ( $0.37 \pm 0.02$ )	$0.94 \pm 0.03$ ( $0.32 \pm 0.09$ )	$0.93 \pm 0.01$ ( $0.26 \pm 0.01$ )
power	$0.94 \pm 0.01$ ( $0.18 \pm 0.00$ )	$0.94 \pm 0.01$ ( $0.18 \pm 0.00$ )	$0.95 \pm 0.01$ ( $0.28 \pm 0.03$ )
wine	none	$0.94 \pm 0.02$ ( $0.49 \pm 0.03$ )	$0.95 \pm 0.02$ ( $0.56 \pm 0.06$ )
yacht	$0.97 \pm 0.04$ ( $0.28 \pm 0.11$ )	$0.93 \pm 0.06$ ( $0.03 \pm 0.01$ )	$0.92 \pm 0.03$ ( $0.03 \pm 0.01$ )
naval	$0.92 \pm 0.01$ ( $0.22 \pm 0.00$ )	$0.96 \pm 0.01$ ( $0.15 \pm 0.25$ )	$0.94 \pm 0.01$ ( $0.03 \pm 0.00$ )
energy	$0.95 \pm 0.02$ ( $0.15 \pm 0.01$ )	$0.94 \pm 0.03$ ( $0.12 \pm 0.18$ )	$0.94 \pm 0.02$ ( $0.05 \pm 0.01$ )
boston	$0.95 \pm 0.03$ ( $0.37 \pm 0.02$ )	$0.94 \pm 0.03$ ( $0.55 \pm 0.20$ )	$0.95 \pm 0.02$ ( $0.34 \pm 0.09$ )
kin8nm	none	$0.93 \pm 0.01$ ( $0.20 \pm 0.01$ )	$0.93 \pm 0.00$ ( $0.20 \pm 0.01$ )

Figure 16: **95% PI PICP and MPIW** The test average and standard deviation PICP of models with validation PICP in [92.5%, 97.5%] is shown, and the test average and standard deviation MPIW is shown in parantheses. “none” indicates the method could not find a model with validation PICP in [92.5%, 97.5%].

This experimental result indicates that:

- Our proposed method (MAQR) is capable of producing PIs that have the correct desired coverage, even in cases when the baseline algorithms are not able to.

- Even when the baseline algorithms do produce PIs with correct desired coverage, *MAQR* produces PIs that are much sharper (e.g. mean PI width for naval dataset is an order of magnitude sharper than all other baselines)

On this limited output and evaluation setting, our proposed method is still competitive in its performance. However, it should be noted that this experiment only tells one small facet of overall UQ quality. Inspecting and evaluating the full predictive uncertainty is necessary for a more thorough evaluation of UQ quality, as done in our main experiments in Section 4.1.

#### B.4 Discussion on Recalibration (Kuleshov et al. [2018])

The recalibration algorithm by Kuleshov et al. [2018] utilizes isotonic regression with a validation set to fine-tune predictive uncertainties from a UQ model. We have applied this recalibration as a post-processing step on the methods presented in Section 4.1, and the empirical results indicate that its effect on overall improvement in UQ quality is inconclusive. Here, we show its effect on one of our methods, *Interval*, because we observe the same pattern across all the methods, including the baseline algorithms.

Recalibration improves average calibration (which is the main focus of the recalibration procedure), but it does so at a cost in sharpness. This is evident in the recalibrated output moving upper left in the average calibration-sharpness plot in Figure 17.

Further, there is little to no improvement in adversarial group calibration (except for the Naval dataset) as shown in Figure 18, which seems to indicate that the improvement in average calibration was not meaningful (i.e. the recalibrated result is not closer to individual calibration). This is also the observation made by Zhao et al. [2020].

At the same time, the proper scoring rules improved on average (Figures B.4, B.4), but interval calibration tended to worsen (Figure B.4).

Based on these metrics, it is difficult to conclude on whether recalibration by Kuleshov et al. [2018] is a beneficial step or not for overall UQ quality. If a practitioner is primarily concerned with average calibration, the results indicate that recalibration *is* a beneficial step, but if converging to the true conditional distribution is the primary objective, recalibration does not seem to be a robust remedy.

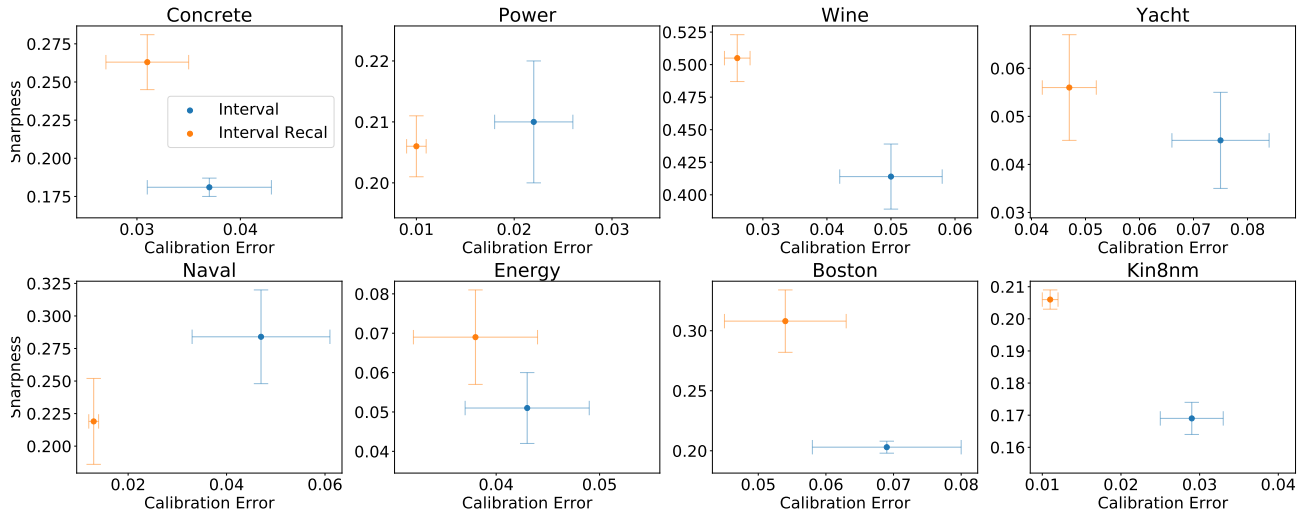


Figure 17: **UCI Average Calibration-Sharpness With Recalibration.** Recalibration tends to trade off sharpness for average calibration.

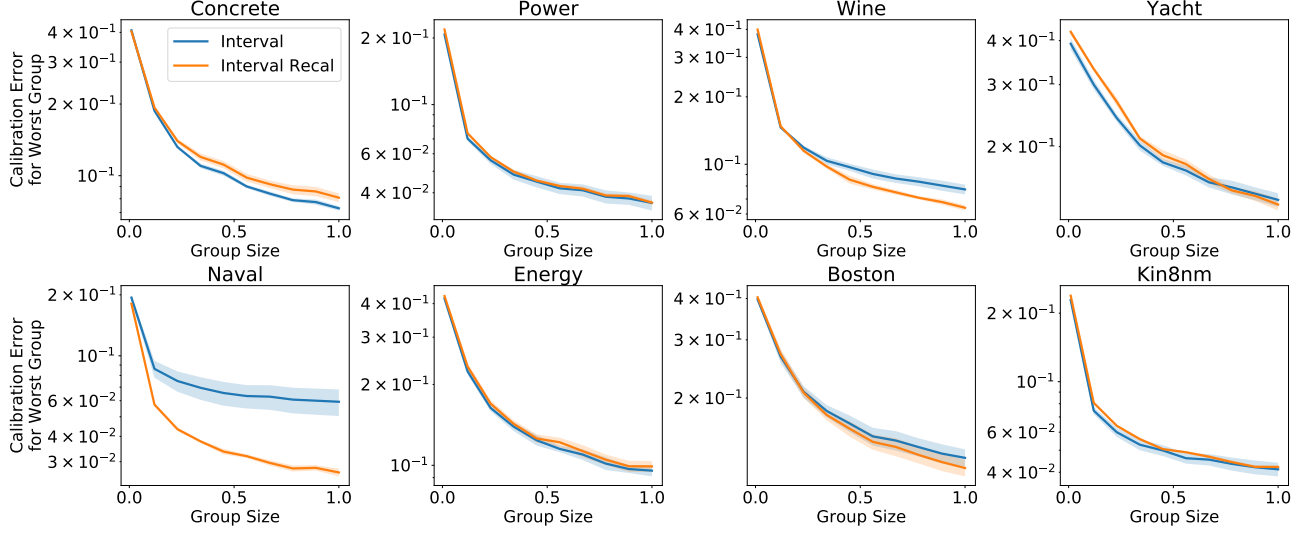


Figure 18: **UCI Adversarial Group Calibration With Recalibration.** Recalibration in general shows little improvement in adversarial group calibration.

	<i>Interval</i>	<i>Interval Recalibrated</i>
concrete	0.086(0.004)	<b>0.077(0.004)</b>
power	0.062(0.001)	<b>0.061(0.001)</b>
wine	0.214(0.006)	<b>0.209(0.013)</b>
yacht	<b>0.018(0.003)</b>	<b>0.018(0.004)</b>
naval	0.066(0.013)	<b>0.062(0.012)</b>
energy	0.017(0.003)	<b>0.016(0.003)</b>
boston	0.094(0.009)	<b>0.076(0.014)</b>
kin8nm	<b>0.077(0.001)</b>	<b>0.077(0.002)</b>

Figure 19: **UCI Check Score with Recalibration.** Recalibration tends to improve the check score.

	<i>Interval</i>	<i>Interval Recalibrated</i>
concrete	0.943(0.053)	<b>0.778(0.064)</b>
power	0.620(0.010)	<b>0.616(0.006)</b>
wine	2.197(0.045)	<b>1.921(0.024)</b>
yacht	0.190(0.021)	<b>0.158(0.025)</b>
naval	<b>3.112(0.053)</b>	3.150(0.050)
energy	0.182(0.026)	<b>0.148(0.028)</b>
boston	1.010(0.118)	<b>0.931(0.107)</b>
kin8nm	0.776(0.017)	<b>0.754(0.023)</b>

Figure 20: **UCI Interval Score with Recalibration.** Recalibration tends to improve the interval score.

	<i>Interval</i>	<i>Interval Recalibrated</i>
concrete	<b>0.061(0.008)</b>	0.068(0.015)
power	<b>0.023(0.003)</b>	0.028(0.008)
wine	<b>0.079(0.014)</b>	<b>0.079(0.019)</b>
yacht	<b>0.121(0.005)</b>	0.136(0.025)
naval	<b>0.043(0.014)</b>	0.105(0.016)
energy	<b>0.060(0.010)</b>	0.066(0.005)
boston	0.079(0.015)	<b>0.078(0.012)</b>
kin8nm	<b>0.048(0.006)</b>	0.061(0.010)

Figure 21: **UCI Interval Calibration with Recalibration.** Recalibration tends to worsen interval calibration.

## C Details on Datasets and Experimental Setup

### C.1 UCI Experiment Details

Here, we provide details on the setup of the UCI experiments presented in Section 4.1.

For each of the 8 UCI datasets, we split 10% of the data into the test set, and we further split 20% of the remaining 90% of the data for the validation, resulting in a train/validation/test split of proportions 72%, 18%, 10%. For all tasks and all 8 datasets, the data was preprocessed by centering to zero mean and scaling to unit variance.

We used the same NN architecture across all methods: 2 layers of 64 hidden units with ReLU non-linearities. We used the same learning rate,  $1e^{-3}$ , and the same batch size, 64, for all methods. For all methods, training was stopped early if the validation loss did not decrease for more than 200 epochs, until a maximum of 10000 epochs. If training was stopped early, the final model was backtracked to the model with lowest validation loss.

*IndvCal* (individual calibration) has one hyperparameter,  $\alpha$ , which balances the NLL loss and the individual calibration loss in the loss function. We 5-fold cross-validated  $\alpha$  in  $[0.0, 1.0]$  in 20 equi-spaced intervals based on Pareto optimality in test set NLL and adversarial group calibration. If there were multiple  $\alpha$  values that were Pareto optimal, we chose the value that had the best test set adversarial group calibration.

*Cali* (penalized calibration loss) has one hyperparameter,  $\lambda$ , which balances the calibration loss and sharpness penalty in the loss function. We tuned  $\lambda$  according to the same grid as above for  $\alpha$ , based on the criterion of adversarial group calibration.

Group batching was applied to *Interval* (interval score) and *Cali* according to the implementation detailed in Appendix C.3. During training, we alternated between “group batching epochs” and “regular batching epochs” (where batches are drawn uniformly from the training set), and the frequency of group batching epochs was a hyperparameter we tuned with cross-validation in  $[0, 1, 3, 5, 10, 30, 100]$ , based on the criterion of adversarial group calibration.

*MAQR* has a two-step training process: we first learn a mean model, then construct a quantile dataset  $D$ , then regress onto this dataset with the quantile model. Both the mean model and the quantile model had the same NN architecture as mentioned above. The mean model was trained with the MSE loss according to the same, aforementioned training procedure. For each UCI dataset, we learned one mean model from the first seed, and re-used this mean model for all other seeds. Using this mean model, we then populated the quantile dataset according to the method outlined in Algorithm 1. Algorithm 1 requires one hyperparameter: the distance threshold in  $\mathcal{X}$  space. We tuned this hyperparameter by setting the minimum distance required to include  $k$  number of points, on average, in constructing an empirical CDF at each training point. We tuned this parameter with cross-validation using the grid  $k \in [10, 20, 30, 40, 50]$ . The quantile model was trained according to the same training procedure but with one difference: the batch size was set to 1024 because the quantile dataset  $D$  could become very large due to many conditional quantile estimates at each training point.

All methods, for all datasets were repeated with 5 seeds:  $[0, 1, 2, 3, 4]$ .



State Variables		Action Variables	
aminor	Minor Radius	pinj_15l	Co-current Beam 1 Power
dssdenest	Line Averaged Electron Density	pinj_15r	Co-current Beam 2 Power
efsbetan	Normalized Beta	pinj_21l	Counter-current Beam 1 Power
efsli	Internal Inductance	pinj_21r	Counter-current Beam 2 Power
efsvolume	Plasma Volume	pinj_30l	Co-current Beam 3 Power
ip	Plasma Curent	pinj_30r	Co-current Beam 4 Power
kappa	Elongation	pinj_33l	Co-current Beam 5 Power
R0	Major Radius	pinj_33r	Co-current Beam 6 Power
tribot	Bottom Triangularity		
tritop	Top Triangularity		

Figure 22: **State and Action Variables for Fusion Dataset.** 10 variables describe the current state of plasma, and the action space is 8 dimensional.

## C.2 Fusion Experiment Details

Here, we first describe the fusion dataset from Section 4.2, then the details of the fusion experiment set up.

The fusion dataset was recorded from the DIII-D tokamak in San Diego, CA, USA, and describes the dynamics of plasma during a nuclear fusion reaction within the tokamak. While the dataset in its raw format is a time-series of the state variables and action variables, for the purposes of a supervised learning problem to learn the dynamics of plasma, it has been re-structrued into a *(state, action, next state)* format. Therefore, the modeling task at hand is to learn the mapping *(state, action)* to *(next state)*, and the UQ task is then to learn the distribution over the next state given the current state and action.

There are 10 plasma state variables that we use both as the input state variables and the target variables. For the action variables, we use the power level of 8 neutral beams, which are a primary means of controlling plasma in a tokamak. These variables are described in Figure 22.

As input to the dynamics model, we model the current state as a 200 millisecond (ms) history window of the 10 state variables and 8 action variables, and we model the current action as a 200ms window into the future of the 8 action variables. The target variables are modeled as the change (or delta) of the state variables 200ms in the future. The state and action features are engineered according to the method used by Fu et al. [2020]. Each 200ms window is taken as one “frame”, the 200ms window is further divided into 2 “frames” of equal length (100ms each), as well as thirds. Then we calculate the mean, variance, and slope of each state and action variable for each of these frames, and collect these statistics as the features. Hence, each 200ms window for 1 variable is summarized into 18 features (3 statistics per frame, and 6 frames per 200ms window). Since there are 10 state variables and 8 action variables, and since the state window is 200ms long and the action window is 200ms long, the input is a 468 dimensional array (10 state variables + 8 previous action variables + 8 current action variables for a total of 26 input variables, and 18 features per variable). Once these features are created, we centered and scaled the inputs and targets to zero mean and unit variance.

There were a total of 100K training data points, and 10K validation and 10K test data points.

The training and hyperparameter tuning procedures were exactly the same as the UCI experiments (detailed above in Appendix C.1), except for two differences: 1) we have increased the NN capacity to 3 hidden layers of 100 hidden units and 2) the batch size was set to 500.

The fusion experiment was likewise repeated 5 times with the seeds [0, 1, 2, 3, 4].

## C.3 Group Batching Implementation Details

Group batching, as introduced in Section 3.4, is a general procedure in which deliberate subsets of the training data are constructed and batched from during train time. There is no “correct” method to form these subsets, because the main point is to simply *not draw batches from  $\mathbb{F}_X$* . One could consider thresholding the values of each dimension of the domain and discretizing the subsets according to the thresholds, and also taking unions of these discretizations to form new subsets as well.

This implementation can be computationally demanding, because for each threshold setting, one has to make sure to choose a subset with sufficiently many points, and iteratively increase or decrease the dimension thresholds if no subset with sufficiently many points can be found. This computational cost increases significantly with dimension.

Our implementation of group batching for all our experiments were as follows: we sort the datapoints according to a single dimension, then take consecutive sets of size equal to the batch size, and use these sets as the batches to take gradient steps over during an epoch. We repeat the above process by cycling through each dimension for sorting. While this process is very simple and inexpensive and only considers a single dimension in constructing the subsets, this group batching scheme has shown to be very effective in our experiments. Group batching in right plot of Figure 1 has also been performed in this exact same way.

#### C.4 Measuring Adversarial Group Calibration

In the main paper, we report adversarial group calibration in right plot of Figure 1, bottom row of Figure 2, and bottom row of Figure 4. The procedure in which we measure adversarial group calibration is the following. For a given test set, we scale group size between 1% and 100% of the full test set size, in 10 equi-spaced intervals, and for each group size, we draw 20 random groups from the test set and record the worst calibration incurred across these 20 random groups.

This is also the method used by Zhao et al. [2020].

### D Considerations for Epistemic Uncertainty

#### D.1 Sources for Epistemic Uncertainty

The primary focus of this paper is on learning a quantile model. For any single setting of the parameters of the quantile model, the model outputs the current best estimate of the *true underlying distribution* of the dataset. Following the notation laid out in Section 2, the learned quantile model  $\hat{\mathbb{Q}}$  is a best approximation to  $\mathbb{Q}$ , the quantile function of the true distribution.

Meanwhile, epistemic uncertainty refers to the uncertainty *in making the distributional prediction*,  $\hat{\mathbb{Q}}$ . Pearce et al. [2018a] provides one method of decomposing the sources of epistemic uncertainty in a regression setting:

- *Model misspecification*:  $\hat{\mathbb{Q}}$  may lack the flexibility to accurately model  $\mathbb{Q}$ , leading to systematic bias.
- *Data uncertainty*:  $\hat{\mathbb{Q}}$  may not be estimated using a representative sample  $\{x_i, y_i\}$  from the assumed underlying distribution.
- *Parameter uncertainty*:  $\hat{\mathbb{Q}}$  may not be estimated using a large enough quantity of samples, leading to uncertainty about the estimated quantity.

Pearce et al. [2018a] has argued that, given the rich class of function approximators at hand today (NN, deep trees, ensembles), model misspecification can be ignored, which we believe is reasonable. In modeling the remaining sources of uncertainties in  $\hat{\mathbb{Q}}$ , we can incorporate common standard methods to quantify epistemic uncertainty, including bootstrapping the data, creating an ensemble of estimates for  $\hat{\mathbb{Q}}$  with random parameter initializations, or fitting a residual process (Liu et al. [2019]). Here, we describe one combination of these methods: an ensemble of estimates of the learned quantile function  $\{\hat{\mathbb{Q}}^{(1)}, \hat{\mathbb{Q}}^{(2)}, \dots\}$  each trained with random initialization (to address parameter uncertainty), on a bootstrapped sample of the training data (to address data uncertainty). The uncertainty over this set of models is the epistemic uncertainty.

#### D.2 Expressing and Utilizing Epistemic Uncertainty

Once we decide on methods to quantify the epistemic uncertainty, the next question is *how to express the epistemic uncertainty*, especially when combining it with the current prediction of the aleatoric uncertainty. This is still an open research question, especially in the regression setting, and methods of combining aleatoric with epistemic uncertainty will differ for how the uncertainty is represented (e.g. density estimates, quantiles, prediction intervals).

One method of combination is to consider the utility of quantifying epistemic uncertainty. Intuitively, for a given input, if we have high epistemic uncertainty, the combined uncertainty should be higher (i.e. less confident prediction), and vice versa. If we consider a single quantile, it is unclear whether lower confidence (due to epistemic uncertainty) would equate to a lower or higher quantile estimate. However, if we consider constructing a centered prediction interval for total uncertainty, it is straightforward to see that lower confidence should widen the interval, by raising the upper bound (quantile level above 0.5) and lowering the lower bound (quantile level below 0.5). This conservative upper and lower bound can be constructed with the bootstrap distribution of each quantile according to each ensemble member prediction. This is also the method utilized in [Pearce et al. \[2018a\]](#).

Suppose we have an ensemble of  $M$  quantile models:  $\{\hat{Q}^{(1)}, \hat{Q}^{(2)}, \dots, \hat{Q}^{(M)}\}$ . For any test point  $x^*$  and test coverage level  $(1 - \alpha^*)$ , the total uncertainty represented by a centered prediction interval with upper bound  $\hat{u}$  and lower bound  $\hat{l}$  is constructed as:

$$\begin{aligned}\hat{l} &= \bar{\mu}(x^*, \alpha^*/2) - z \frac{s(x^*, \alpha^*/2)}{\sqrt{M}} \\ \hat{u} &= \bar{\mu}(x^*, 1 - \alpha^*/2) + z \frac{s(x^*, 1 - \alpha^*/2)}{\sqrt{M}} \\ \bar{\mu}(x^*, p^*) &= \frac{1}{M} \sum_{i=1}^M \hat{Q}^{(i)}(x^*, p^*) \\ s(x^*, p^*) &= \sqrt{\frac{1}{M-1} \sum_{i=1}^M (\hat{Q}^{(i)}(x^*, p^*) - \bar{\mu}(x^*, p^*))^2}\end{aligned}$$

and  $z$  is the chosen critical value (e.g. 1.96 for a conservative bound that takes the 95% confidence interval of the bootstrap distribution). In words, the construction of  $\hat{u}, \hat{l}$  equates to constructing a conservative prediction interval that depends on how dispersed or concentrated each ensemble member’s predictions are.

### D.3 Metrics for Total Uncertainty Evaluation

After choosing a method to express epistemic uncertainty and combining it with aleatoric uncertainty for a prediction of total uncertainty, next comes the question of *how to evaluate the combined uncertainty*.

The critical point here is that the calibration, sharpness and proper scoring rule metrics we have discussed thus far *are not applicable here*. This is because these metric only judge how close the prediction is to the true underlying distribution. In fact, ECE (a measure of average calibration) can be shown to be identical to the Wasserstein distance between distributions under the  $L1$  distance metric ([Zhao et al. \[2020\]](#)). In a hypothetical setting where we have very few datapoints and hence very high epistemic uncertainty throughout the whole data support, if one distributional prediction was extremely lucky and predicted a distribution that adheres exactly to the true underlying distribution, the aforementioned metrics will consider this prediction a perfect prediction – however, a lucky guess is not at all a useful UQ, and to a practitioner, a less confident prediction (by quantifying high epistemic uncertainty) is much more useful, rather than a very confident prediction that can be correct if it is lucky, but confidently very incorrect otherwise.

We also emphasize here that, while standard evaluation experiments and metrics exist for the *classification* setting (e.g. by training an image classifier on the MNIST dataset and testing on the Non-MNIST dataset to assess the entropy of the predicted class probabilities or the output of a trained out-of-distribution detector), there does not exist standard experiments and metrics to evaluate epistemic uncertainty in the *regression setting*.

Therefore, we propose one evaluation metric to assess combined total uncertainty, which is *sharpness subject to sufficient coverage* and we will refer to this metric as “epistemic coverage”. Epistemic coverage measures average calibration of a centered prediction interval, but the difference in observed probabilities from expected probabilities is penalized only when the observed probability is less than the expected probability (i.e. do not penalize the prediction if the observed probability is higher than the expected probability), and if this sufficient coverage condition is met, then we evaluate sharpness.

By this metric, only over-confidence is penalized and under-confidence is considered acceptable. However, since infinitely wide prediction intervals are also not useful, we also consider sharpness after sufficient coverage is met.

#### D.4 Demonstrating Effect of Bootstrap Ensembling and the Epistemic Coverage Metric

We design an “epistemic experiment” to show the effect of incorporating epistemic uncertainty via bootstrapped ensembles. In this experiment, we swap the train and test sets, such that the training set is much smaller than the test set (roughly  $\frac{1}{7}$  of test set size), hence, the model should have very high epistemic uncertainty in making predictions on the test set. It is expected that by not incorporating epistemic uncertainty in such a setting, the model will produce *overconfident* predictions that are *too sharp*. This overconfidence will be penalized heavily by the epistemic coverage metric we described above in Appendix D.3, and sharpness should also indicate that the predictions are too tight. Producing conservative distributional predictions via the bootstrapped ensembling technique described above in Appendix D.2 is expected to mitigate these overconfidence issues by incorporating epistemic uncertainty.

We show the effect on one of our methods, *Interval*, because the same effect can be observed for any of the quantile methods, including the baseline algorithms. The results are shown in Figure 23.

When a conservative PI is constructed with the bootstrapped ensemble (labelled *Interval Boot-Ens*), the epistemic coverage error decreases significantly to or near zero, which is expected given that the conservative bounds only work to widen the PI, and the epistemic coverage error only penalizes PI that are not wide enough. The increase in width is also evident in the increase in sharpness with bootstrap ensembling.

Therefore, the ensembling technique does work to incorporate epistemic uncertainty from a practical standpoint by imbuing more underconfidence into the distributional predictions. Still, quantifying and evaluating epistemic uncertainty in a regression setting is an open problem, and we leave for future work developing alternative methods of quantifying epistemic uncertainty in regression.

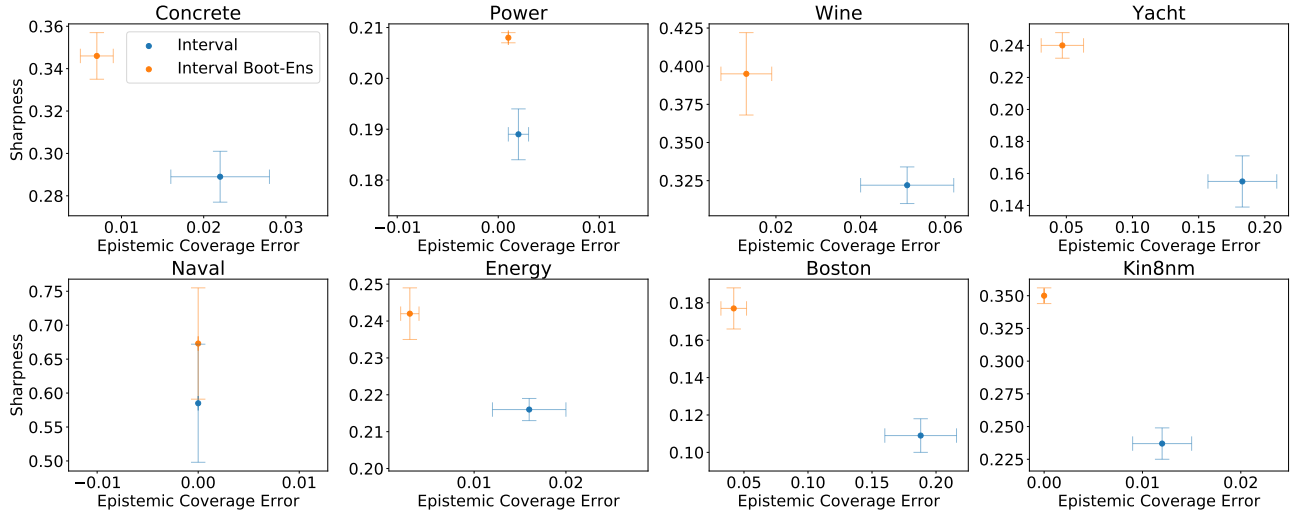


Figure 23: **Epistemic Experiments on UCI Datasets.** We evaluate epistemic coverage in the epistemic experiment setting where the train set is much smaller than the test set. Epistemic coverage only penalizes overconfidence. Sharpness is the average width of the 95% PI.